Quantum Spin Liquids

V.R. Shaginyan

Petersburg Nuclear Physics Institute, Gatchina, Russia

Euler Symposium, July 12-17, 2013, St. Petersburg

Exotic quantum spin liquid (QSL) is made with such hypothetic particles as fermionic spinons which carry spin 1/2 and no charge. A great variety of QSL are discovered in theory. The experimental identifying of QSLs heavily depends on theoretical interpretation making the search for the corresponding material to investigate spin liquid a challenge in condensed matter physics.

Mineral Herbertsmithite $ZnCu_3(OH)_6Cl_2$ is an insulator

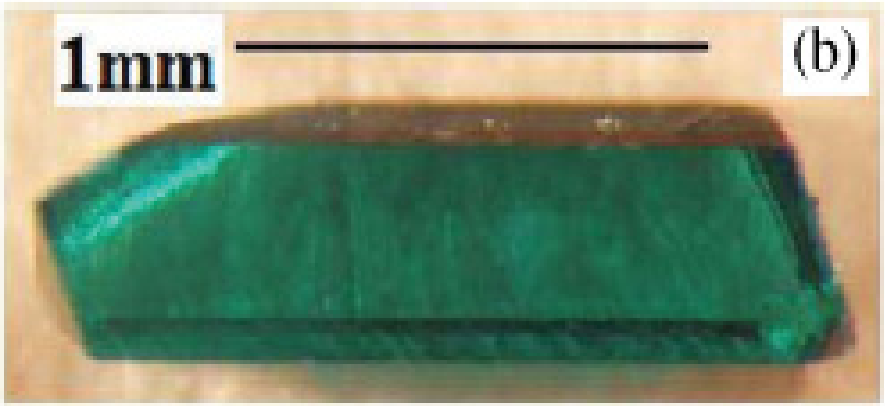

T.T. Han et.al.,
PRB 83, 100402 (2011).

We show that:

Mineral Herbertsmithite represents a fascinating experimental example when new particles-spinons, non-existing as free ones, dominate its properties at low temperatures.

Caused by the spin-charge separation the low-temperature thermodynamic, heat transport and relaxation properties of the insulator herbertsmithite are similar to those of metals rather than of insulators.

Herbertsmithite is a new type of strongly correlated electrical insulator that possesses properties of heavy fermion metals with one exception: it resists the flow of electric charge.

(Herbertsmithite) $ZnCu_3(OH)_6Cl_2$.

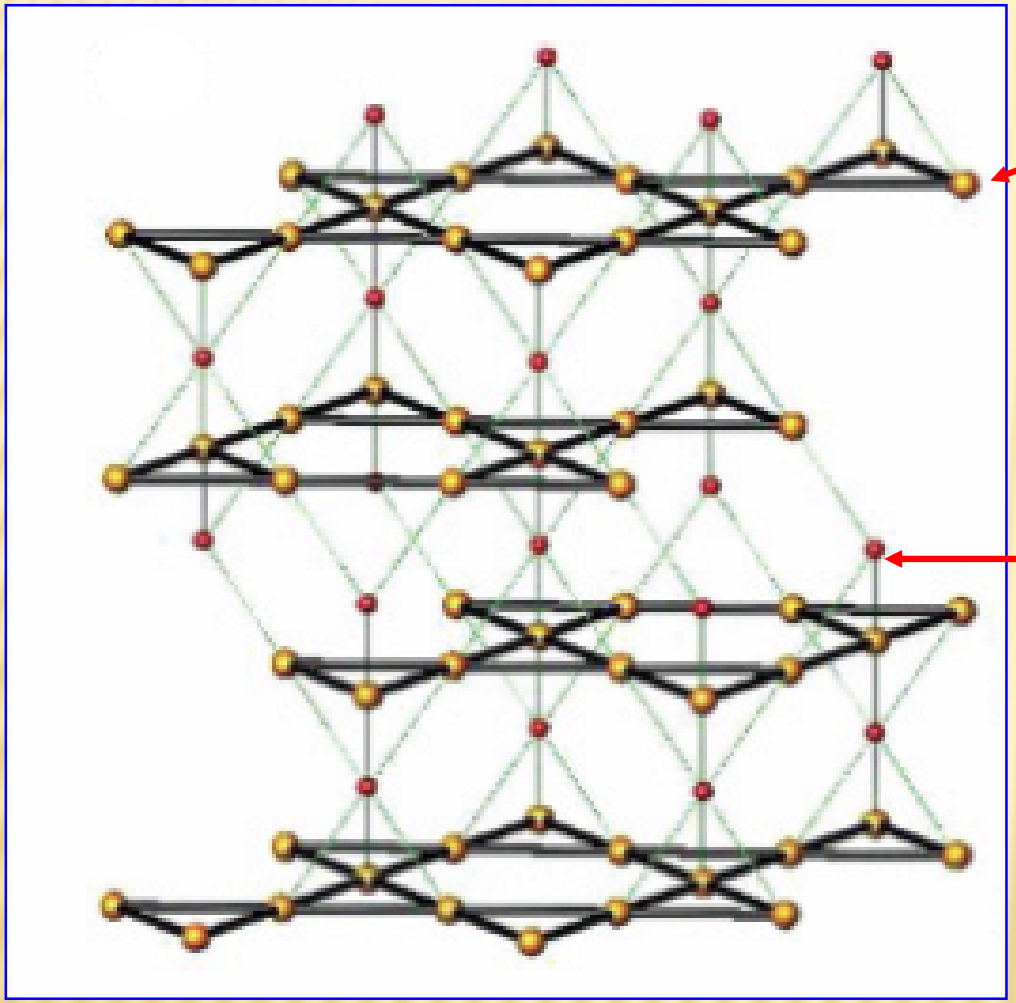

Cu2+(large brown spheres)

Zn2+(small red spheres)

T. H. Han *et al.*, Phys. Rev. B **83**, 100402(R) (2011).

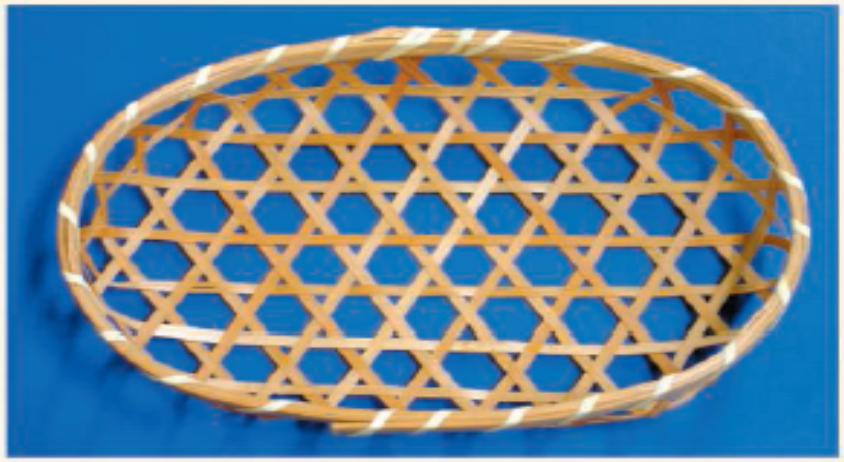

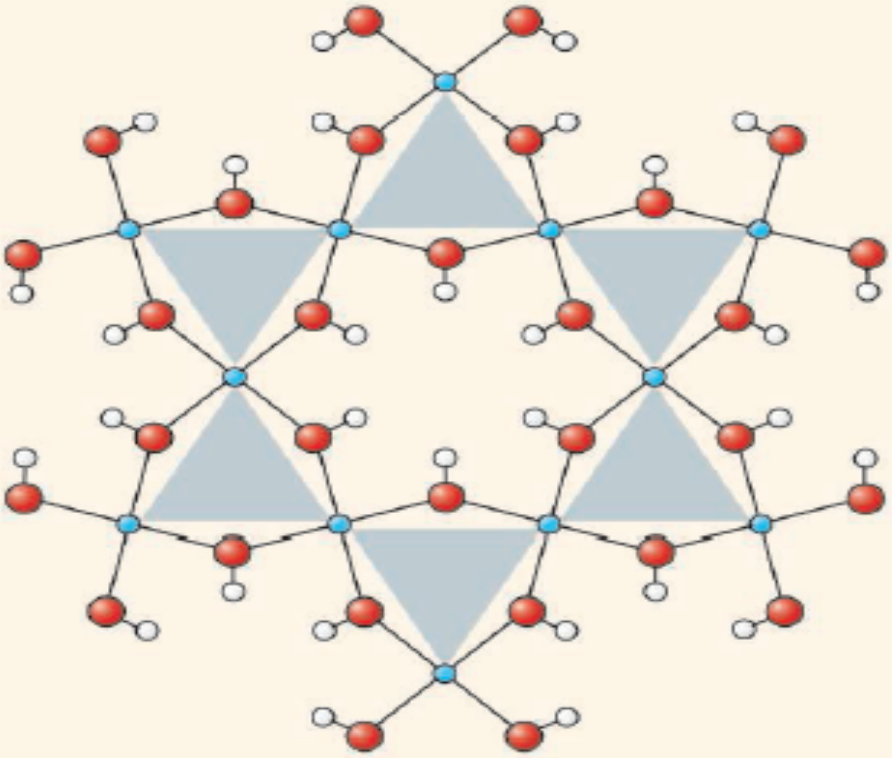

Meeting with frustration. (**Top**) A Kagome basket. (**Bottom**) Structure of $ZnCu_3(OH)_6Cl_2$ (*10*) showing that the Cu ions (blue) occupy a Kagome lattice; O-H is red-white.

Tian-Heng Han et al., **Nature, December 2012, "Fractionalized excitations in the spin-liquid state of a kagome-lattice antiferromagnet"**

The experimental realization of quantum spin liquids is a long sought goal in physics, as they represent new states of matter. A key feature of spin liquids is that they support exotic spin excitations carrying fractional quantum numbers. However, detailed measurements of these ‘fractionalized excitations’ have been lacking. Neutron scattering measurements on single-crystal samples of the spin-1/2 kagome-lattice antiferromagnet called herbertsmithite, provide striking evidence for this characteristic feature of spin liquids. At low temperatures, the spin excitations form a continuum, in contrast to the conventional spin waves expected in ordered antiferromagnets.

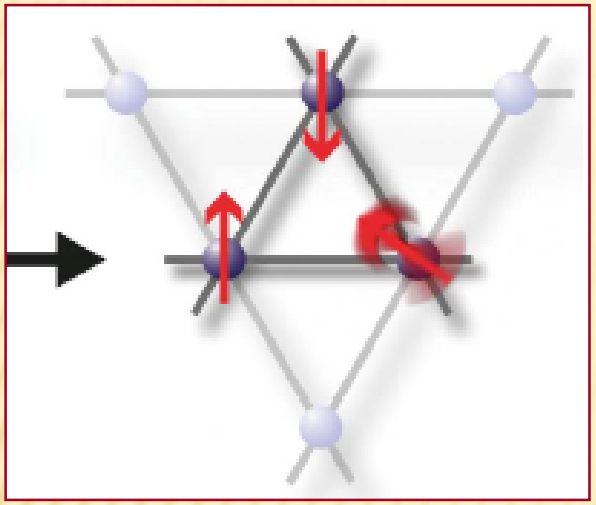

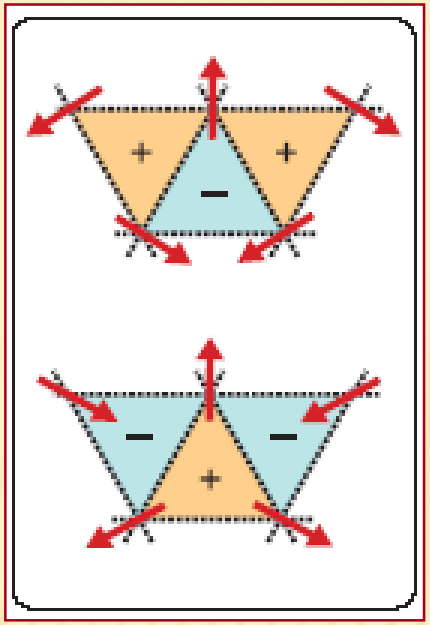

The lattice is "frustrated" because if an up- and down-spin occupy two corners of a triangle, the spin on the third corner does not know which way to point to obtain the lowest-energy configuration.

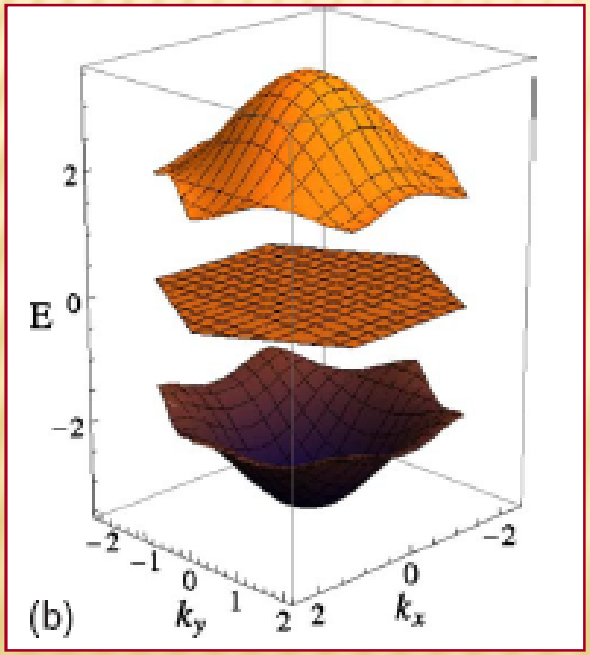

JETP Lett. 94 252 (2011)

Flat bands in topological media

T. T. Heikkilä *1), *N. B. Kopnin*+, *G. E. Volovik*+

PHYSICAL REVIEW B **82**, 075104 (2010)

Isolated flat bands and spin-1 conical bands in two-dimensional lattices

Dmitry Green,[1,*] Luiz Santos,[2] and Claudio Chamon[3]

Normal Fermi liquid and Fermi liquid with the flat band are separated by Fermion Condensation Quantum Phase Transition (FCQPT)

Normal Fermi liquid

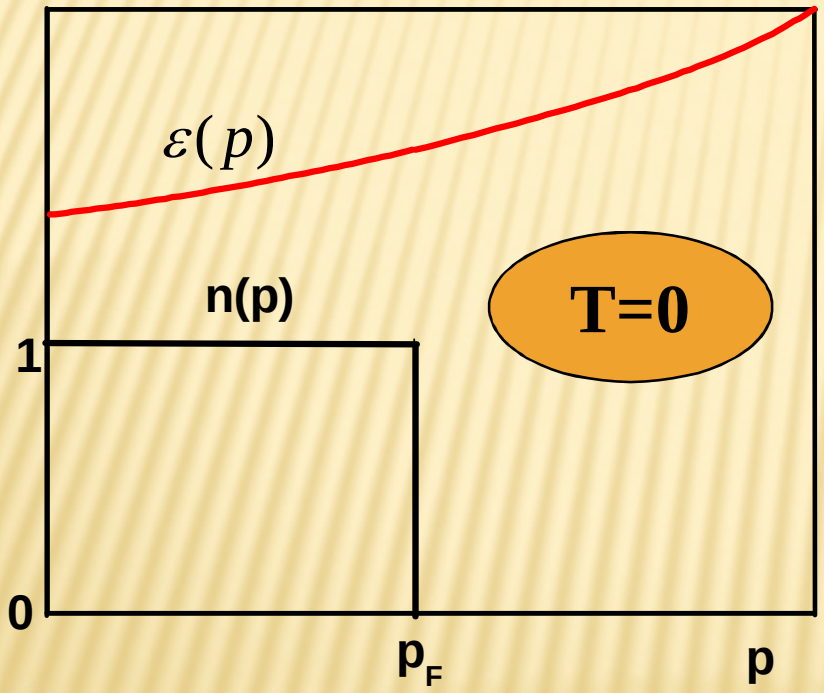

Fermi liquid with a flat band

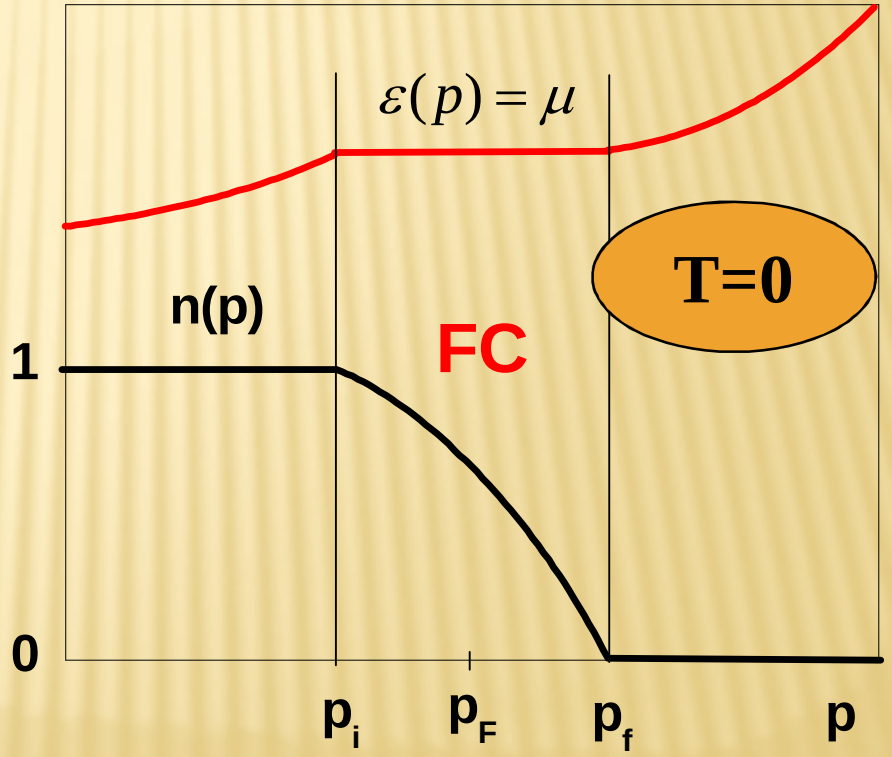

V. A. Khodel and V. R. Shaginyan, JETP Lett. 51, 553 (1990)

V. R. Shaginyan, M. Ya. Amusia, A. Z. Msezane, and K. G. Popov, Phys. Rep. 492, 31 (2010)

THE LANDAU EQUATION FOR THE EFFECTIVE MASS M*

$$\frac{1}{M^*(T,B)} = \frac{1}{M^*} + \int \frac{\vec{p}_F \vec{p}}{{p_F}^3} f(p_F, p) \frac{\partial\,[n(p,T,B) - n_0(p)]}{\partial p} \frac{d\,\vec{p}}{(2\pi)^3}.$$

$$M^*_{LFL} = const.$$

$$S(T) = aM^*T, \quad C(T) = bM^*T.$$

At FCQPT the band is flat and M* is infinite, while the equation becomes homogeneous, and is solved analytically

$$\frac{1}{M^*(T,B)} = \int \frac{\vec{p}_F \vec{p}}{{p_F}^3} f(p_F, p) \frac{\partial\,[n(p,T,B) - n_0(p)]}{\partial p} \frac{d\,\vec{p}}{(2\pi)^3}.$$

$$M^*(B) \propto B^{-2/3}. \qquad M^*(T) \propto T^{-3/2}.$$

$$\frac{1}{M^*(T,B)} = \int \frac{\vec{p}_F \vec{p}}{p_F^3} f(p_F, p) \frac{\partial\,[n(p,T,B) - n_0(p)]}{\partial p} \frac{d\vec{p}}{(2\pi)^3}.$$

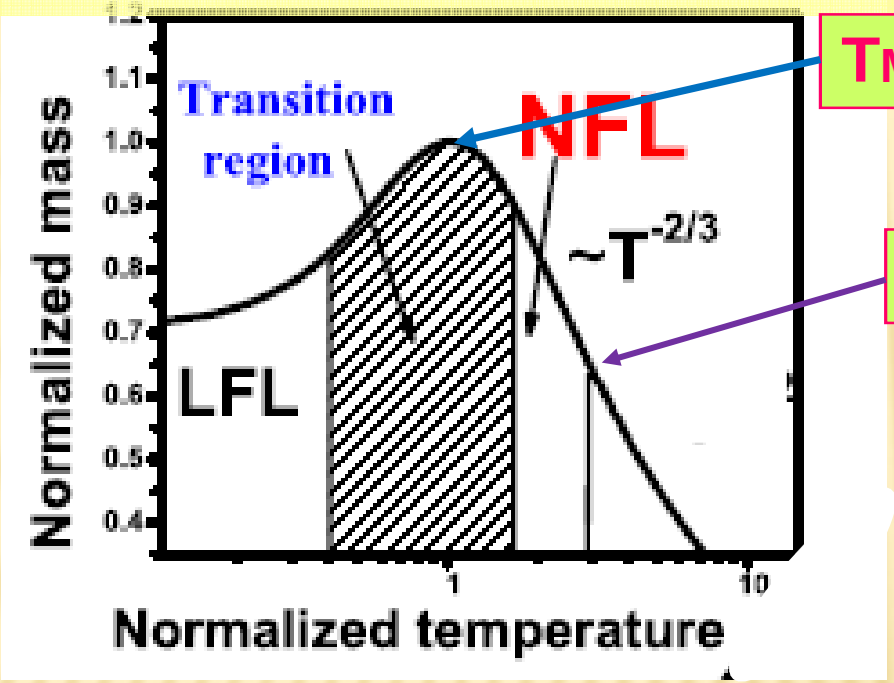

T_M

Inflection point T*

An approximate solution of the Landau equation when the effective mass M* tends to infinity.

$$M^*_M(B) \propto (B)^{-2/3}; T_M \propto B. \qquad M^*(T) \propto T^{-2/3}.$$

$$M^*_N(y) = \frac{M^*(T,B,x)}{M^*_M} \approx \frac{1 + c_1 y^2}{1 + c_2 y^{8/3}}; y = \frac{T}{T_M}.$$

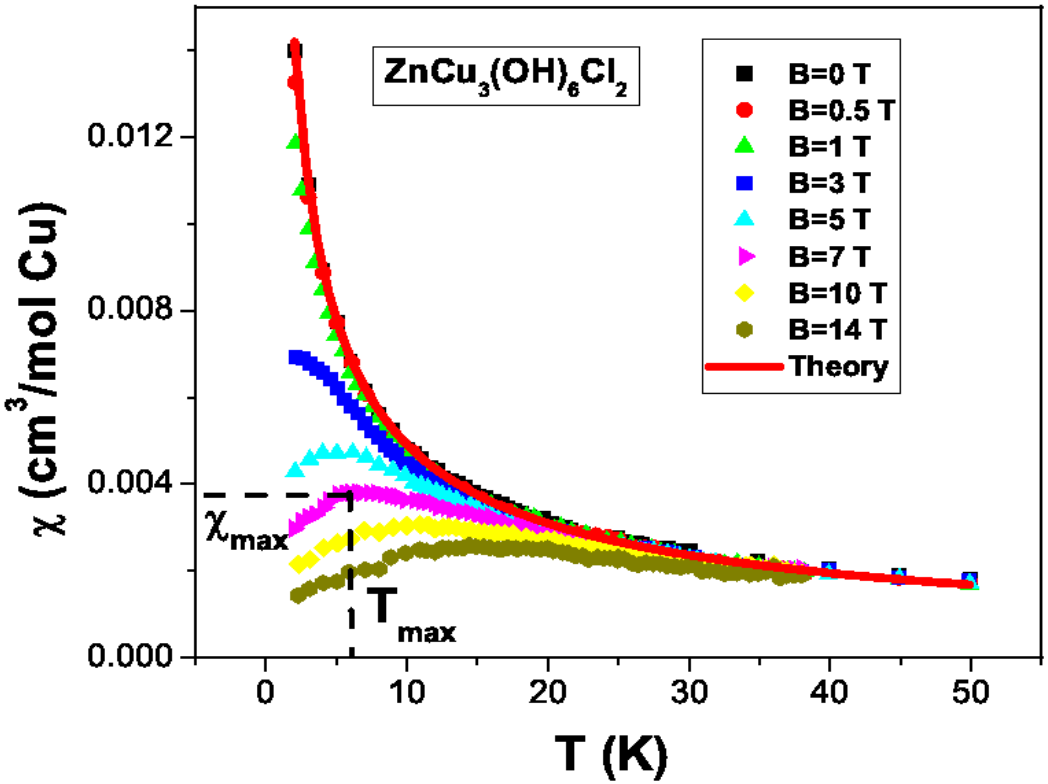

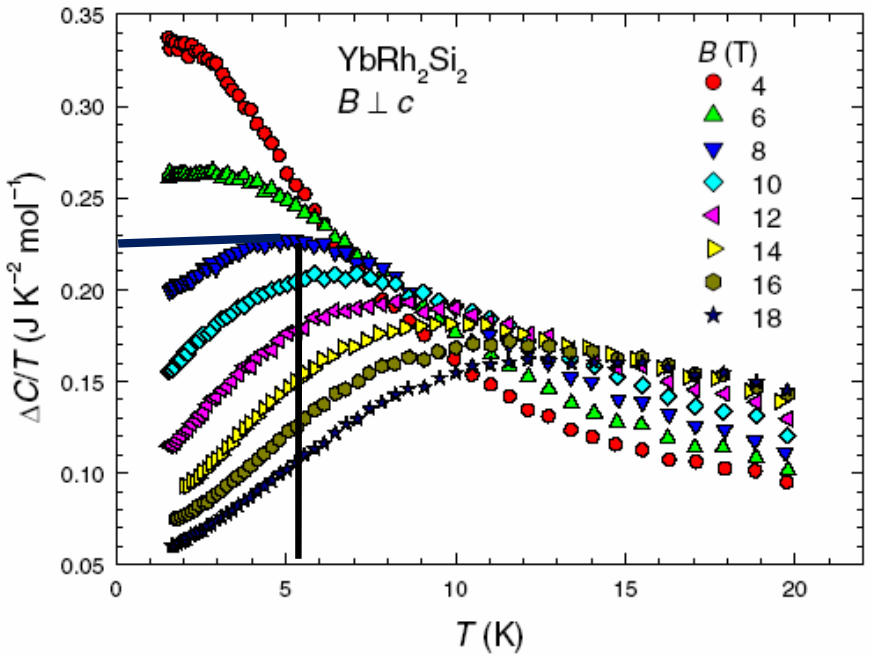

FIG. 1: Temperature dependence of the magnetic susceptibility χ at different magnetic fields for $ZnCu_3(OH)_6Cl_2$[8]. The illustrative values of χ_{max} and T_{max} at $B = 7$ T are also shown. Our calculations made at $B = 0$ are depicted by the solid curve representing $\chi(T) \propto T^{-\alpha}$ with $\alpha = 2/3$.

J.S. Helton *et al.*, Phys. Rev. Lett. **104**, 147201 (2010).

V. R. Shaginyan, M. Ya. Amusia, A. Z. Msezane, and K. G. Popov, Phys. Rep. **492**, 31 (2010).

free fitting parameters. The normalized effective mass $M_N^* = M^*/M_M^*$ as a function of the normalized temperature $y = T_N = T/T_{\max}$ is given by the interpolating function[2,16]

$$M_N^*(y) \approx c_0 \frac{1 + c_1 y^2}{1 + c_2 y^{8/3}}. \qquad (4)$$

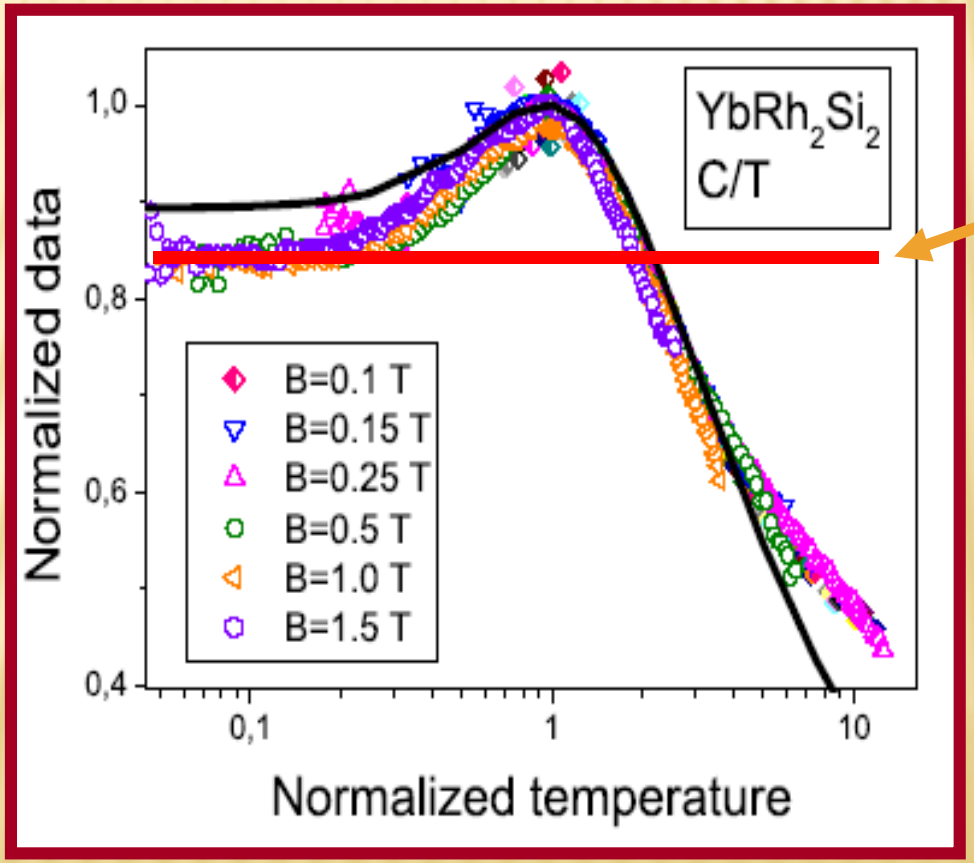

LFL

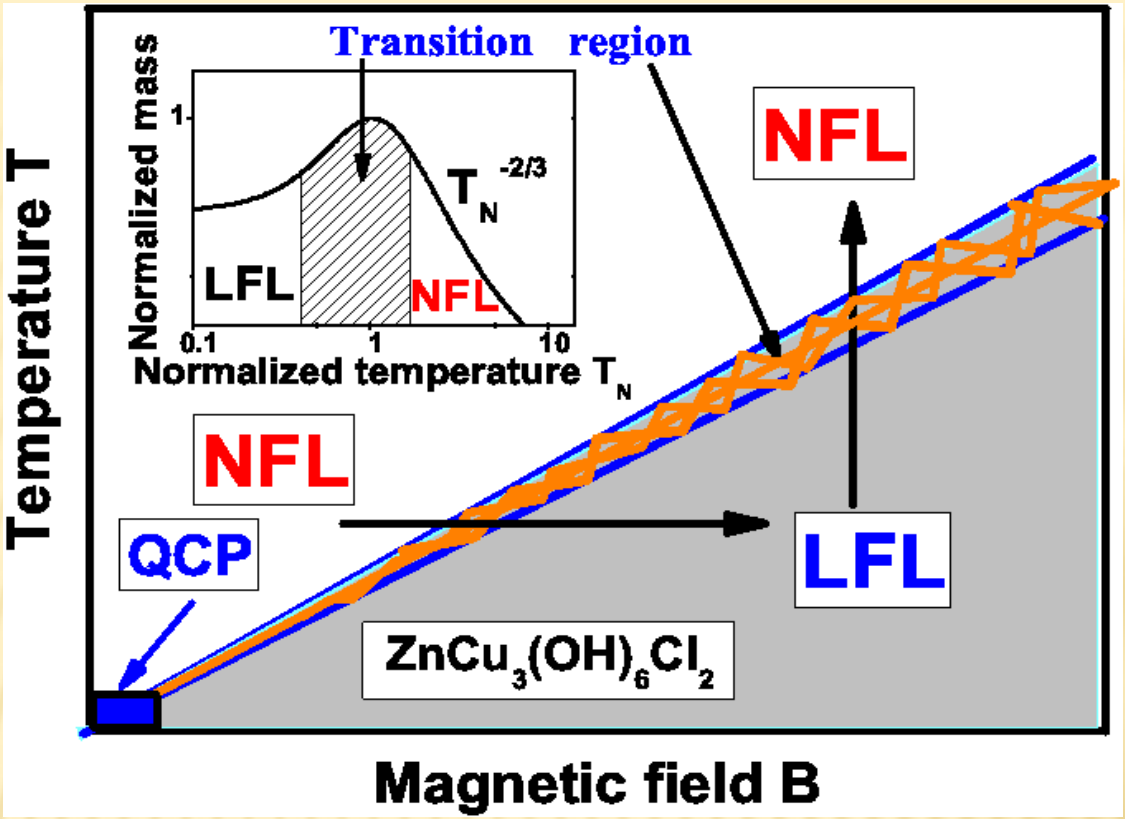

FIG. 2: Schematic phase diagram of $ZnCu_3(OH)_6Cl_2$. The vertical and horizontal arrows show LFL-NFL and NFL-LFL transitions at fixed B and T respectively. Inset shows a schematic plot of the normalized effective mass versus the normalized temperature. Transition region, where M_N^* reaches its maximum at $T_N = T/T_{\max} = 1$, is shown by the arrows and hatched area in both the main panel and in the inset.

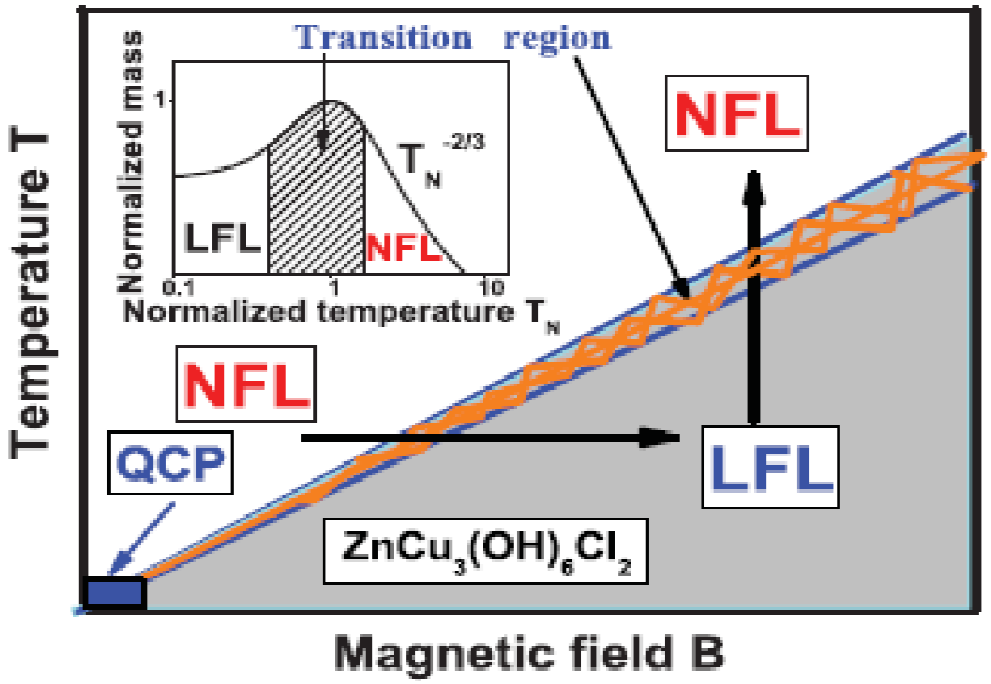

FIG. 2. (Color online) Phase diagram of $ZnCu_3(OH)_6Cl_2$. The vertical and horizontal arrows show LFL-NFL and NFL-LFL transitions at fixed B and T, respectively. The inset shows a plot of the normalized effective mass vs the normalized temperature. The transition region, where M_N^* reaches its maximum at $T_N = T/T_{\max} = 1$, is shown by the arrows and the hatched area in both the main panel and in the inset.

$$M^*_N(y) = \frac{M^*(T,B,x)}{M^*_M} \approx \frac{1+c_1 y^2}{1+c_2 y^{8/3}}; y = \frac{T}{T_M}.$$

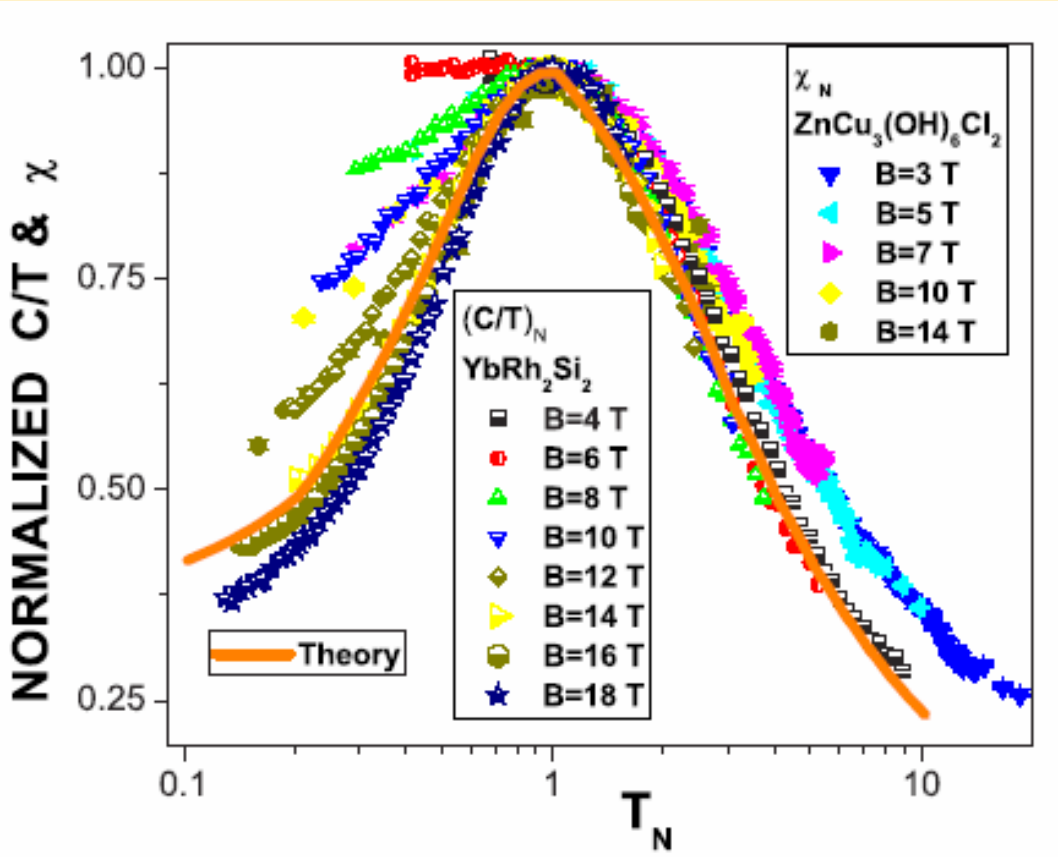

FIG. 3: Normalized susceptibility $\chi_N = \chi/\chi_{\max} = M_N^*$ versus normalized temperature T_N. χ_N is extracted from the measurements of the magnetic susceptibility χ in magnetic fields[8] B shown in Fig. 1. Normalized specific heat $(C/T)_N = M_N^*$ is extracted from the measurements of C/T on $YbRh_2Si_2$ in magnetic fields[22] B. The corresponding fields B are listed in the legends. Our calculations made at field B completely polarizing the quasiparticle band are depicted by the solid curve tracing the scaling behavior of M_N^*.

V. R. Shaginyan, A. Z. Msezane, and K. G. Popov, Phys. Rev. B 84, 60401(R) (2011)

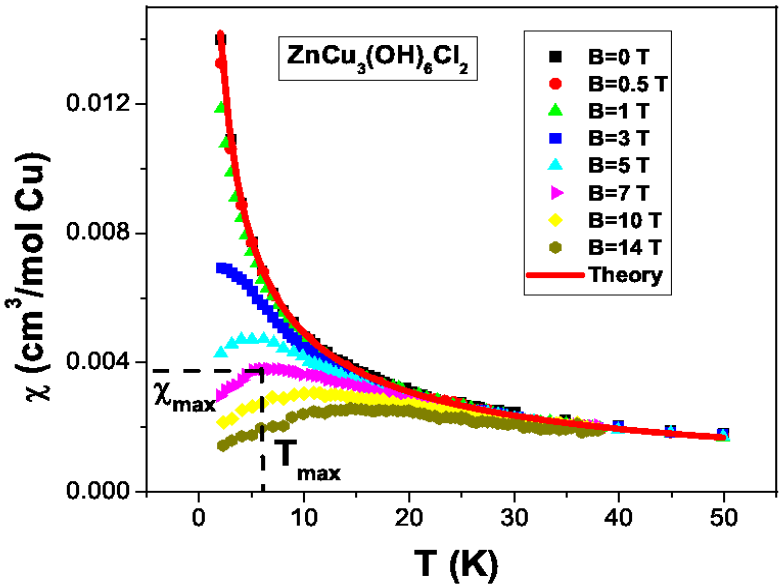

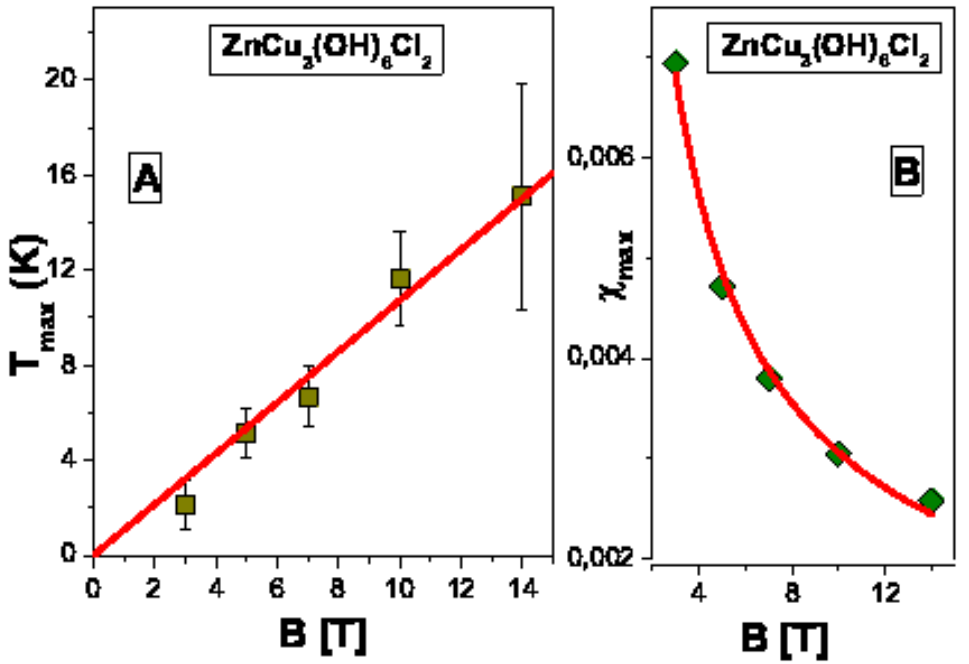

FIG. 5: Panel **A**: The temperatures $T_{\max}(B)$ at which the maxima of χ (see Fig. 1) are located. The solid line represents the function $T_{\max} \propto aB$, a is a fitting parameter, see Eq. (5). Panel **B**: The maxima $\chi_{\max}$ of the function $\chi(T)$ versus magnetic field B (see Fig. 1). The solid curve is approximated by $\chi_{\max}(B) = dB^{-2/3}$, see Eq. (3), d is a fitting parameter.

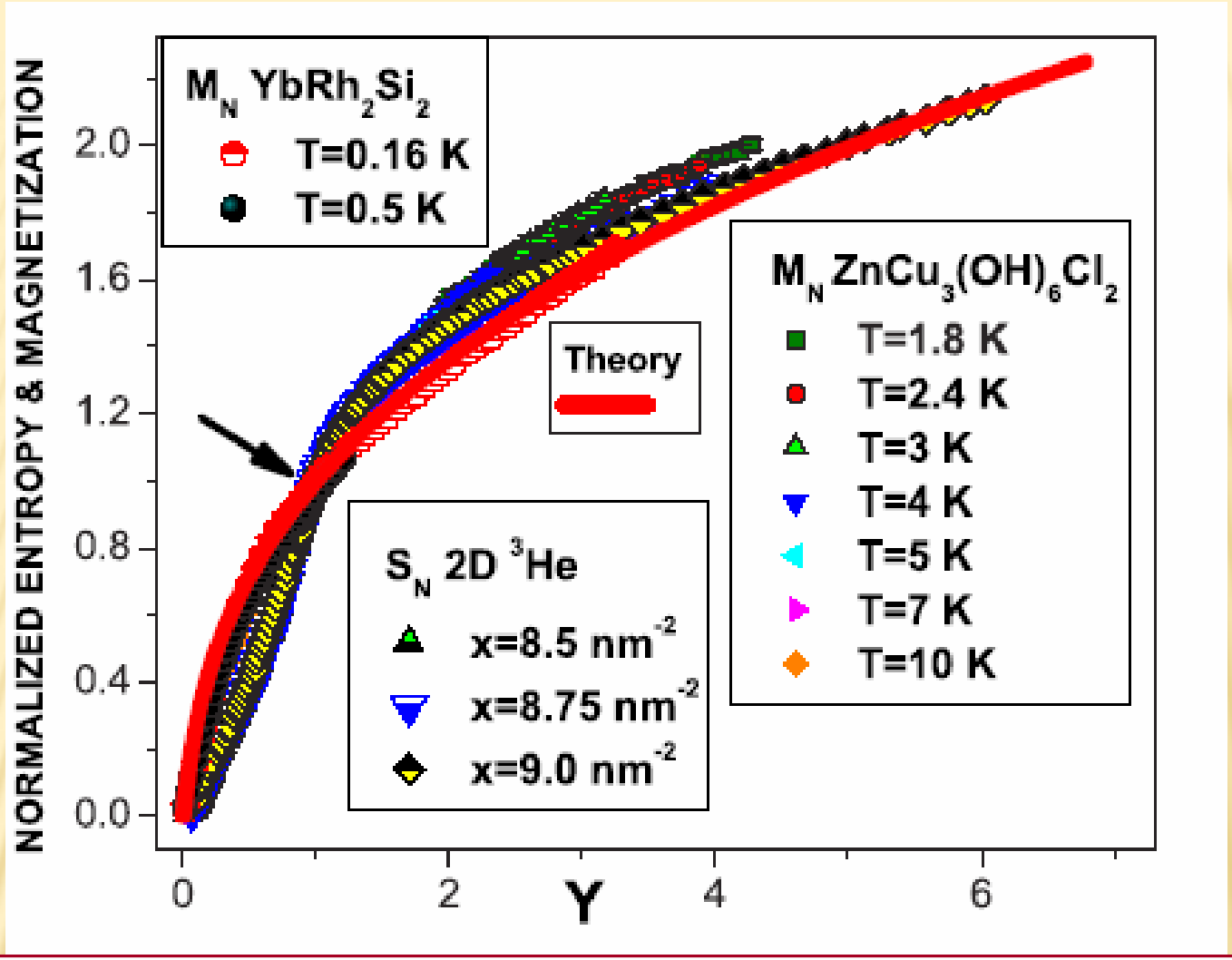

Y=T/Tk

Y=B/Bk

FIG. 4: Normalized magnetization $M_N(y)$ collected on measurements on $ZnCu_3(OH)_6Cl_2$[8] and $YbRh_2Si_2$[23] at different temperatures shown in the corresponding legends. Shown by the arrow a kink is clearly seen at $y \simeq 1$. The normalized entropy $S_N(y)$ is extracted from measurements on 2D ^3He[3] at different densities x shown in the legend. The solid curve represents our calculations of the normalized magnetization.

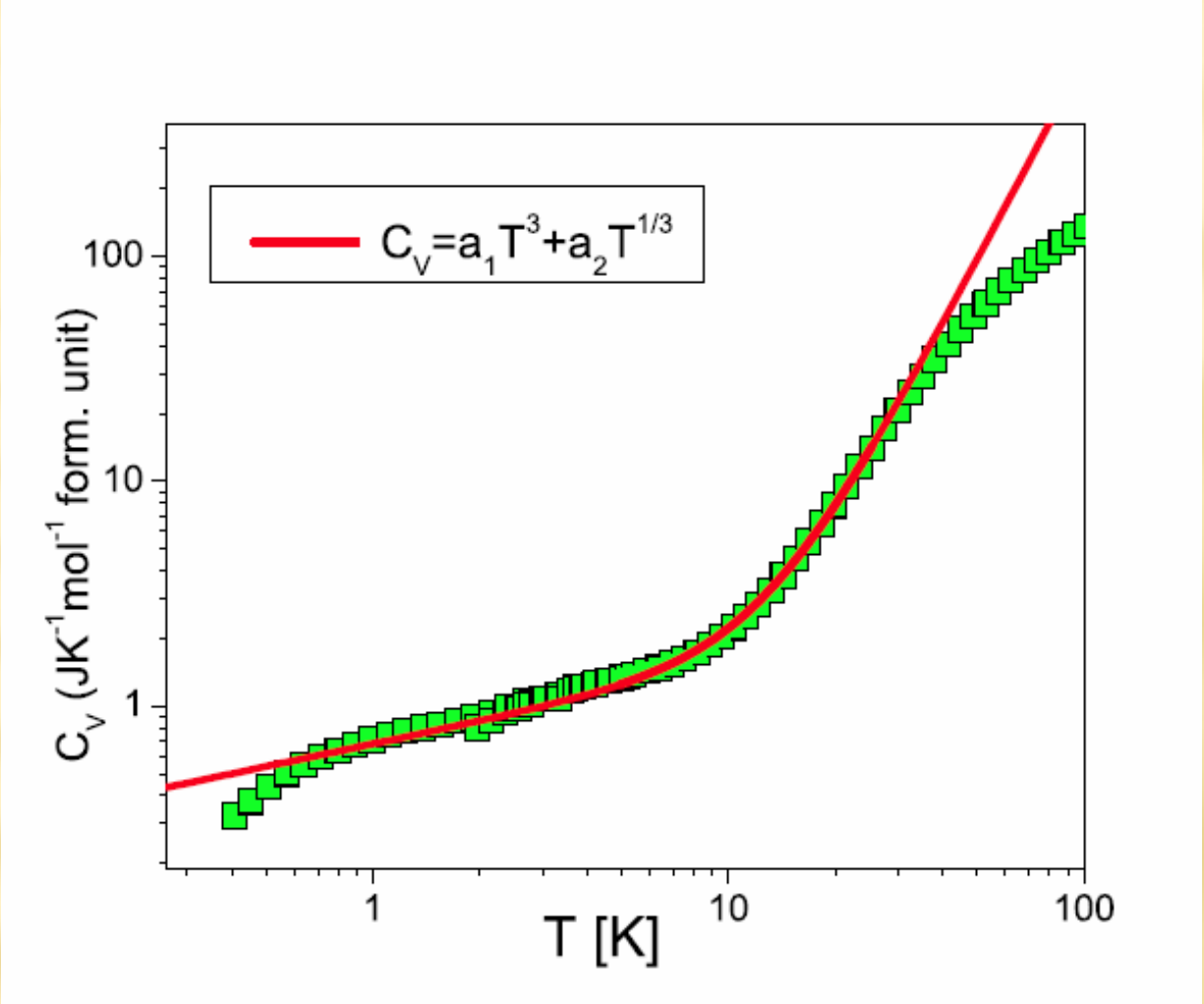

Specific heat versus T in ZnCu3(OH)6Cl2 .

M. A. deVries, K. V. Kamenev, W. A. Kockelmann, J. Sanchez-Benitez, and A. Harrison Phys. Rev. Lett. **100**, 157205 (2008).

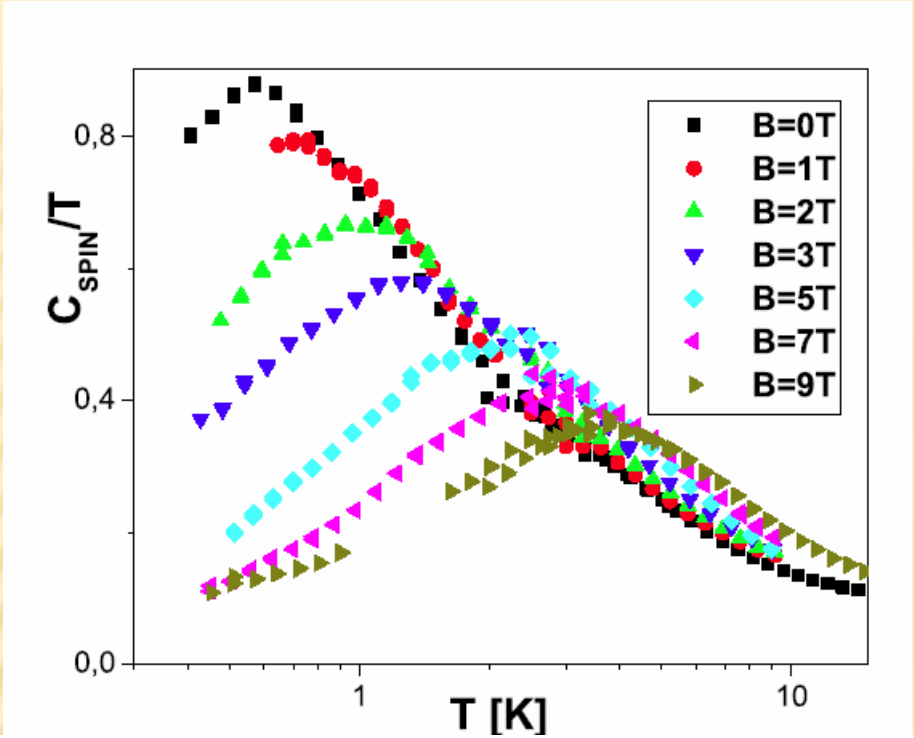

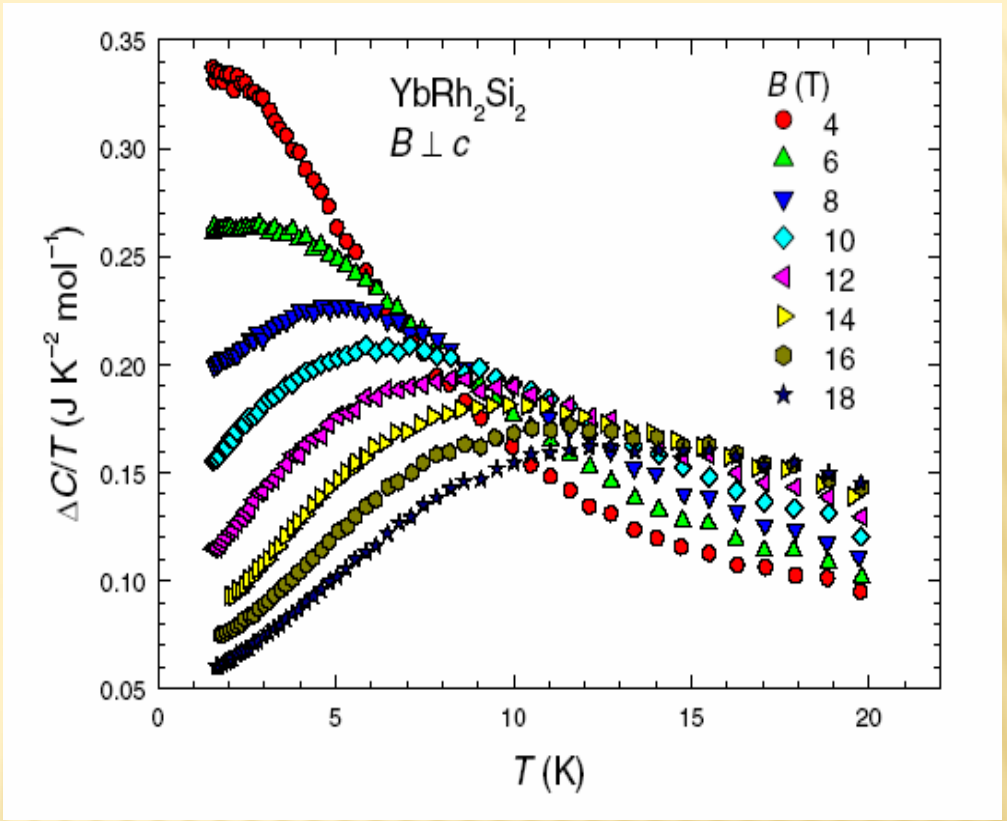

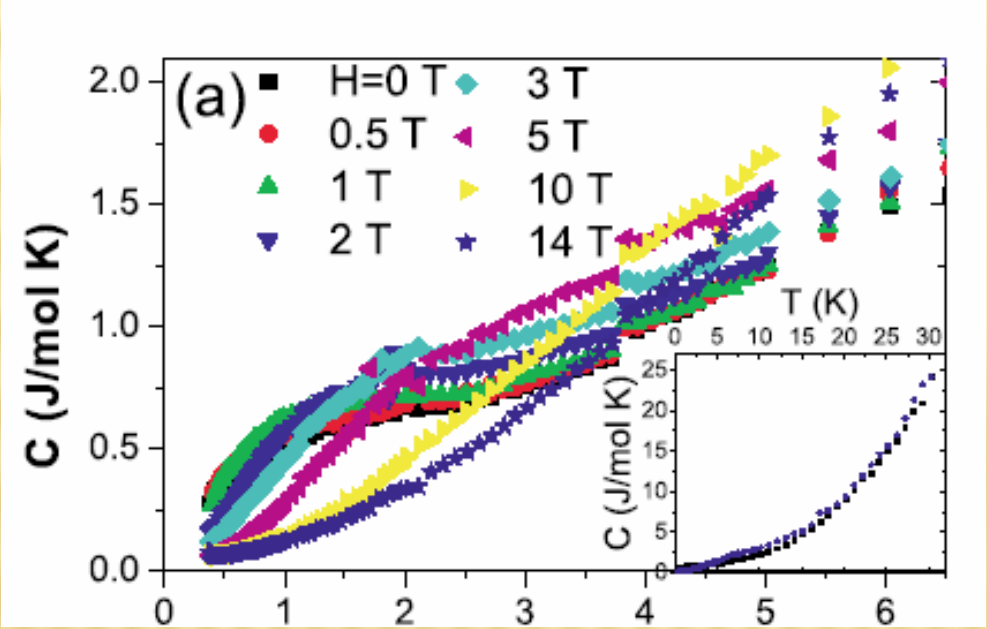

$C_{spin}=C - C_{phonon}$

$$C_{phonon} \propto T^3, C_{spin} \propto T.$$

The specific heat Cspin(B,T)/T versus magnetic field B measured on ZnCu3(OH)6Cl2 as a function of temperature.

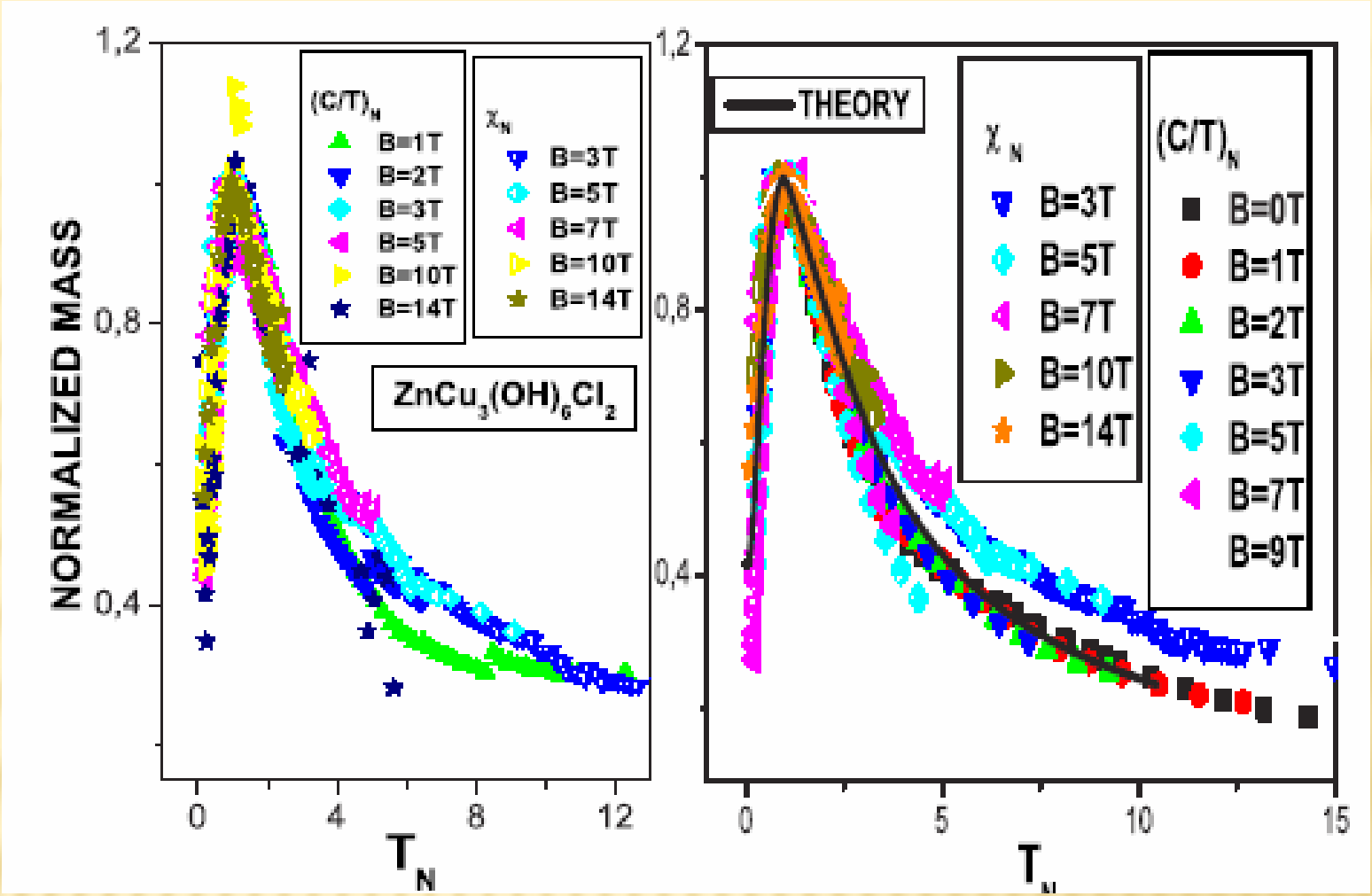

The normalized specific heat Cspin(B,T)/T and susceptibility versus magnetic field B measured on ZnCu3(OH)6Cl2 as a function of temperature.

V.R. Shaginyan, A.Z. Msezane, K.G. Popov, G.S. Gaparidze, V.A. Stephanovich, Identification of Spin Liquid, Europhys. Lett. , Europhys. Lett. 97, 56001 (2012).

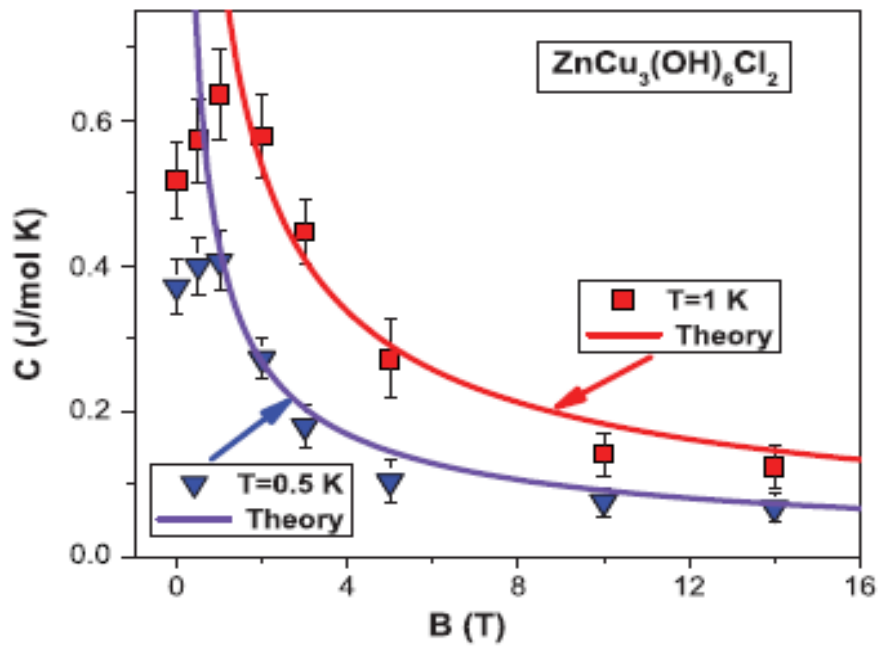

FIG. 6. (Color online) The specific heat $C(B,T)$ vs magnetic field B measured on $ZnCu_3(OH)_6Cl_2$ at two different temperatures (Ref. 6) T listed in the legends is shown by the triangles and squares. Our calculations are depicted by the solid curves, tracing the LFL behavior of $C(B,T) = a_1 B^{-2/3} T$ [see Eq. (3)], with a_1 being a parameter.

The heat capacity C(T)/T as a function of B.

$$S(T) = aT, \quad C(T) = bT.$$

$$M^*(B) \propto (B - B_c)^{-2/3}.$$

PHYSICAL REVIEW B 84, 060401(R) (2011)

Thermodynamic properties of the kagome lattice in herbertsmithite

V. R. Shaginyan,[1,2] A. Z. Msezane,[2] and K. G. Popov[3]

Spin-lattice relaxation rate of quantum spin liquid

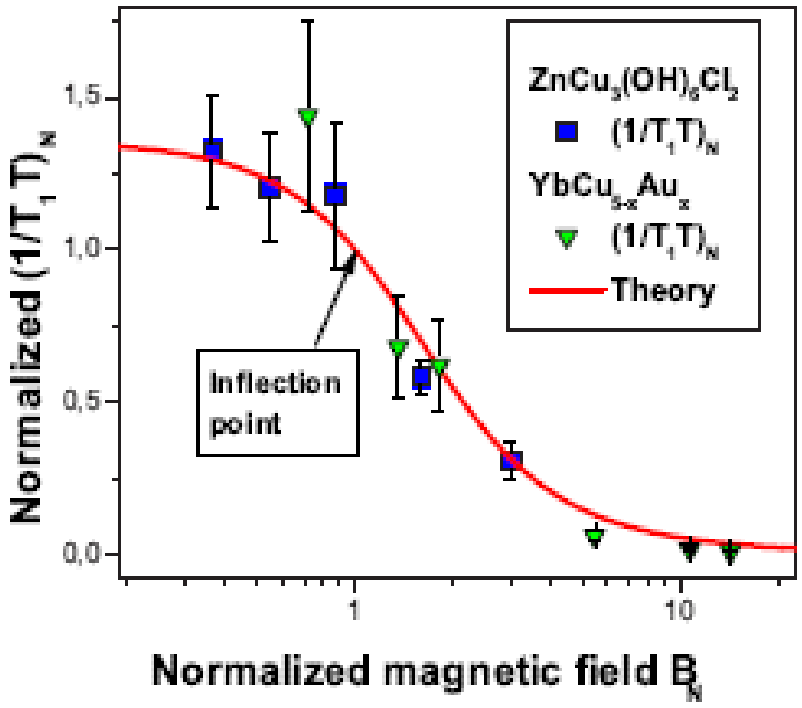

Fig. 8: The relaxation properties of herbertsmithite versus those of HF metals. The normalized spin-lattice relaxation rate $(1/T_1T)_N$ at fixed temperature as a function of magnetic field: Solid squares correspond to data on $(1/T_1T)_N$ extracted from measurements on $ZnCu_3(OH)_6Cl_2$ [26], while the solid triangles correspond to those extracted from measurements on $YbCu_{5-x}Au_x$ with $x = 0.4$ [27]. The inflection point where the normalization is taken is shown by the arrow. Our calculations based on eq. (1) are depicted by the solid curve tracing the scaling behavior of $(M_N^*)^2$.

$$\frac{1}{T_1T} = \frac{3}{4\mu_B^2}\sum_{\mathbf{q}} A_{\mathbf{q}}A_{-\mathbf{q}}\frac{\chi''(\mathbf{q},\omega)}{\omega}\bigg|_{\omega\to 0} \propto (M^*)^2$$

Dependence of spin-lattice relaxation rate at various magnetic fields and at fixed temperature in HF metal YbCu4.4Au0.6 and ZnCu3(OH)6Cl2.

P. Carretta et al., PR B **79**, 020401R, 2009; T. Imai et al., PRL **100**, 077203 (2008).

V.R. Shaginyan, A.Z. Msezane, K.G. Popov, G.S. Gaparidze, V.A. Stephanovich, Identification of Spin Liquid, Europhys. Lett. 97, 56001 (2012).

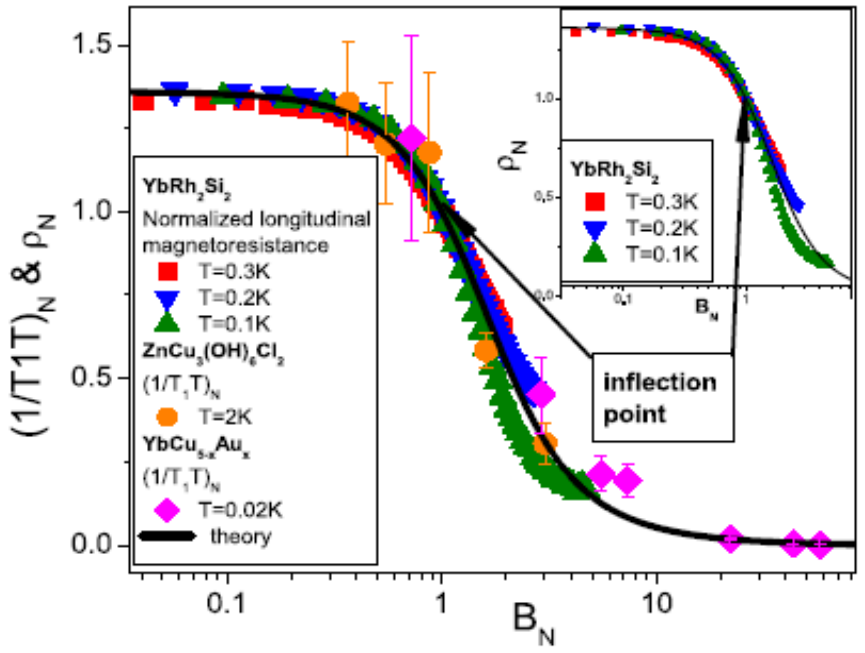

Fig. 3. (Color online.) Magnetic field dependence of normalized (see text for details) muon spin-lattice relaxation rate $(1/T_1T)_N$ extracted from measurements on $YbCu_{4.4}Au_{0.6}$ [29] and $ZnCu_3(OH)_6Cl_2$ [30] along with the normalized longitudinal magnetoresistance ρ_N versus normalized magnetic field B_N. Our calculations are shown by the solid line. The arrows indicate the inflection points. Inset: ρ_N versus B_N, ρ_N is extracted from measurements on $YbRh_2Si_2$ at different temperatures [31] listed in the legend. The solid curve represents our calculations.

$$\frac{1}{T_1T} = \frac{3}{4\mu_B^2}\sum_{\mathbf{q}} A_{\mathbf{q}}A_{-\mathbf{q}}\frac{\chi''(\mathbf{q},\omega)}{\omega}\bigg|_{\omega\to 0} \propto (M^*)^2$$

$$\rho_N(B_N) = \frac{\rho(B_N)-\rho_0}{\rho_{inf}} = \left(\frac{1}{T_1T}\right)_N = (M_N^*)^2$$

QSL in the organic compound

The organic insulator EtMe3Sb[Pd(dmit)2]2.

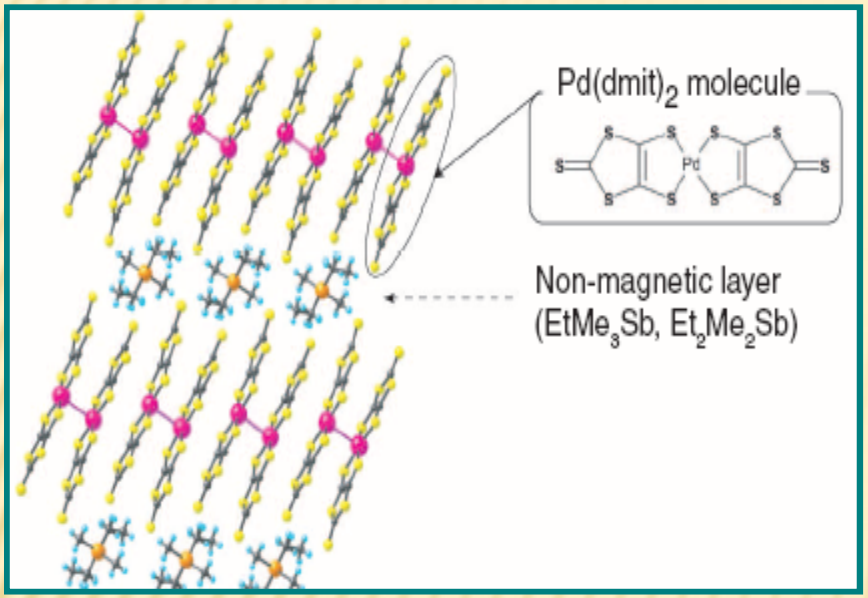

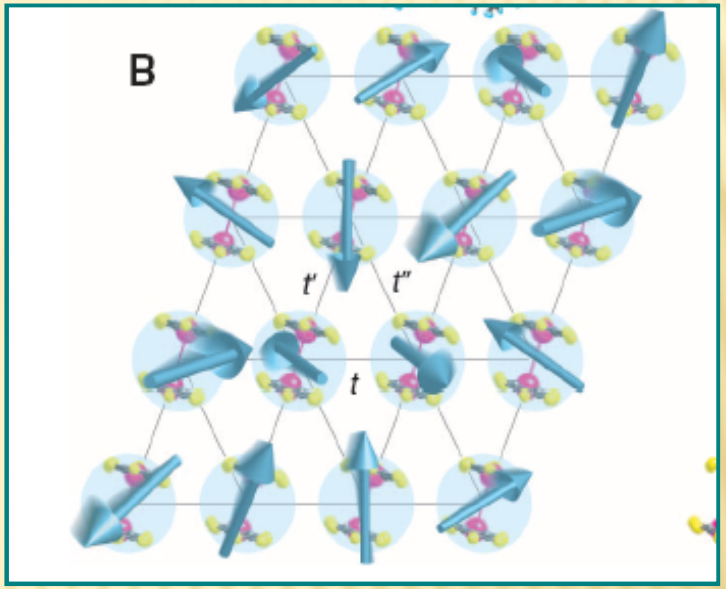

Fig. 1. The crystal structure of $EtMe_3Sb[Pd(dmit)_2]_2$ and $Et_2Me_2Sb[Pd(dmit)_2]_2$. (**A**) A view parallel to the 2D magnetic $Pd(dmit)_2$ layer, separated by layers of a nonmagnetic cation. (**B**) The spin structure of the 2D planes of $EtMe_3Sb[Pd(dmit)_2]_2$ (dmit-131), where Et = C_2H_5, Me = CH_3, and dmit = 1,3-dithiole-2-thione-4,5-dithiolate. $Pd(dmit)_2$ are strongly dimerized (table S1), forming spin-1/2 units $[Pd(dmit)_2]_2^-$ (blue arrows). The antiferromagnetic frustration gives rise to a state in which none of the spins are frozen down to 19.4 mK (4). (**C**) The spin structure of the 2D planes of

H. M. Yamamoto, N. Nakata, Y. Senshu, M. Nagata, H. M. Yamamoto, R. Kato, T. Shibauchi, and Y. Matsuda, Science **328**, 1246 (2010).

Thermal Transport

EtMe3Sb[Pd(dmit)2]2
k-(BEDT-TTF)2Cu2(CN)3
are likely to host QSL

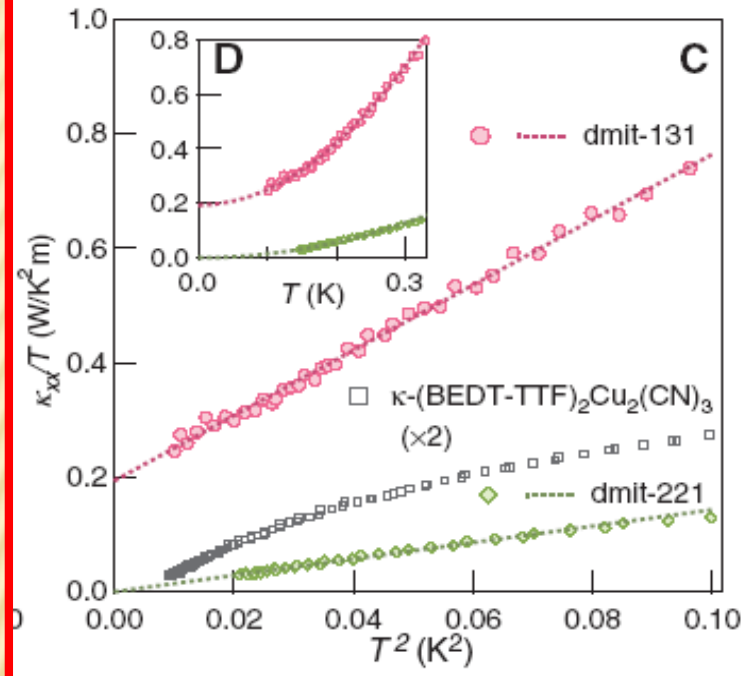

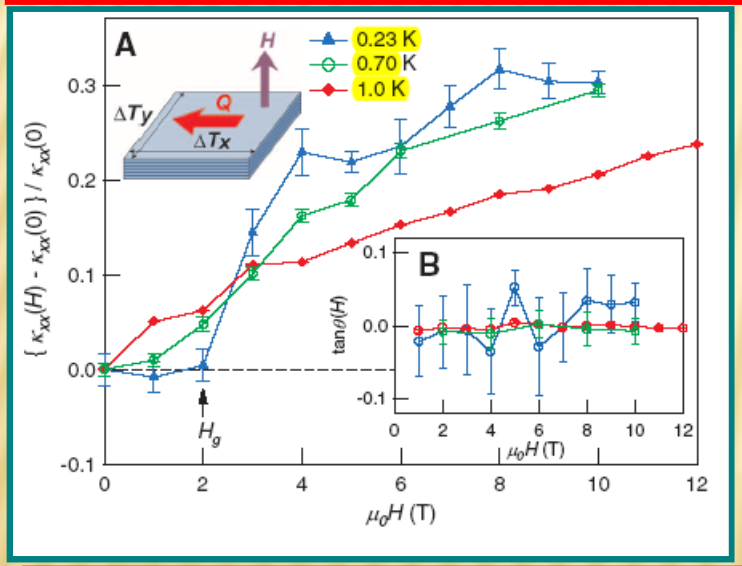

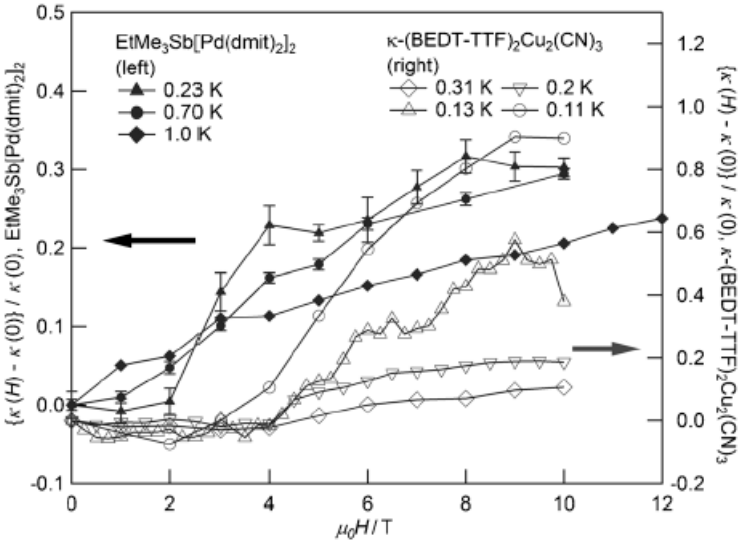

Figure 3. Field dependence of κ. The change under field normalized by the zero-field value is plotted.

Fig. 3. (**A**) Field dependence of thermal conductivity normalized by the zero field value, $[\kappa_{xx}(H) - \kappa_{xx}(0)]/\kappa_{xx}(0)$ of dmit-131 at low temperatures. (Inset) The heat current ***Q*** was applied within the 2D plane, and the magnetic field ***H*** was perpendicular to the plane. κ_{xx} and κ_{xy} were determined by diagonal and off-diagonal temperature gradients, ΔT_x and ΔT_y, respectively.

H. M. Yamamoto, N. Nakata, Y. Senshu, M. Nagata, H. M. Yamamoto, R. Kato, T. Shibauchi, and Y. Matsuda, Science **328**, 1246 (2010).

M. Yamashita, T. Shibauchi, and Y. Matsuda, ChemPhysChem **13**, 74 (2012).

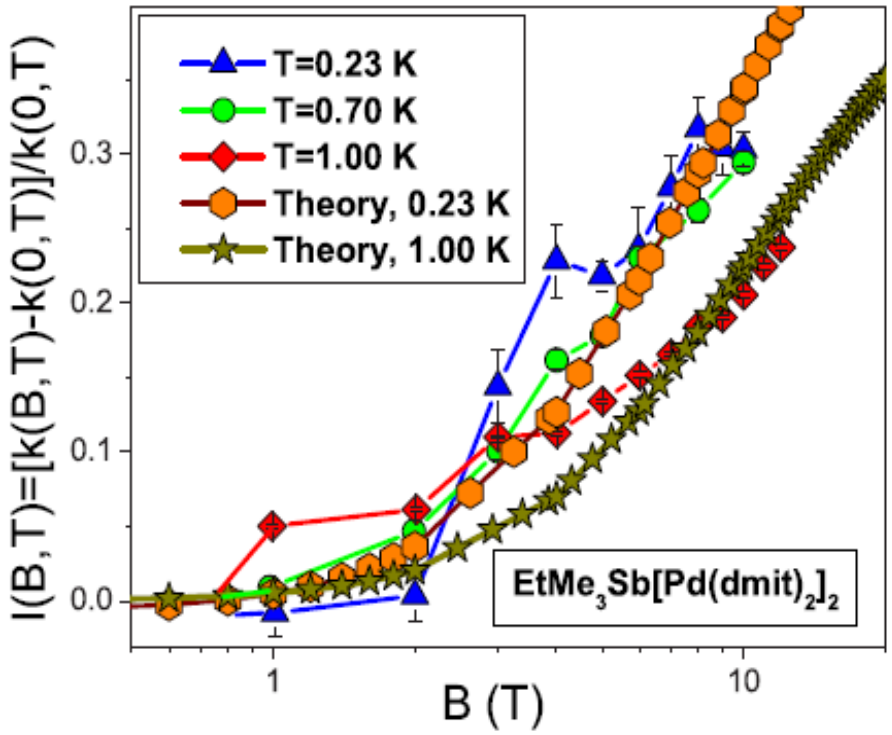

FIG. 13: Magnetic field B dependence of normalized thermal conductivity $I(B,T)$ measured on the organic insulator $EtMe_3Sb[Pd(dmit)_2]_2$ and standardized by the zero field value κ, $I(B,T) = [\kappa(B,T) - \kappa(B=0,T)]/\kappa(B=0,T)$ at temperatures shown in the legend [50, 51]. Our calculations are based on Eq. (14) and shown by pentagons and stars.

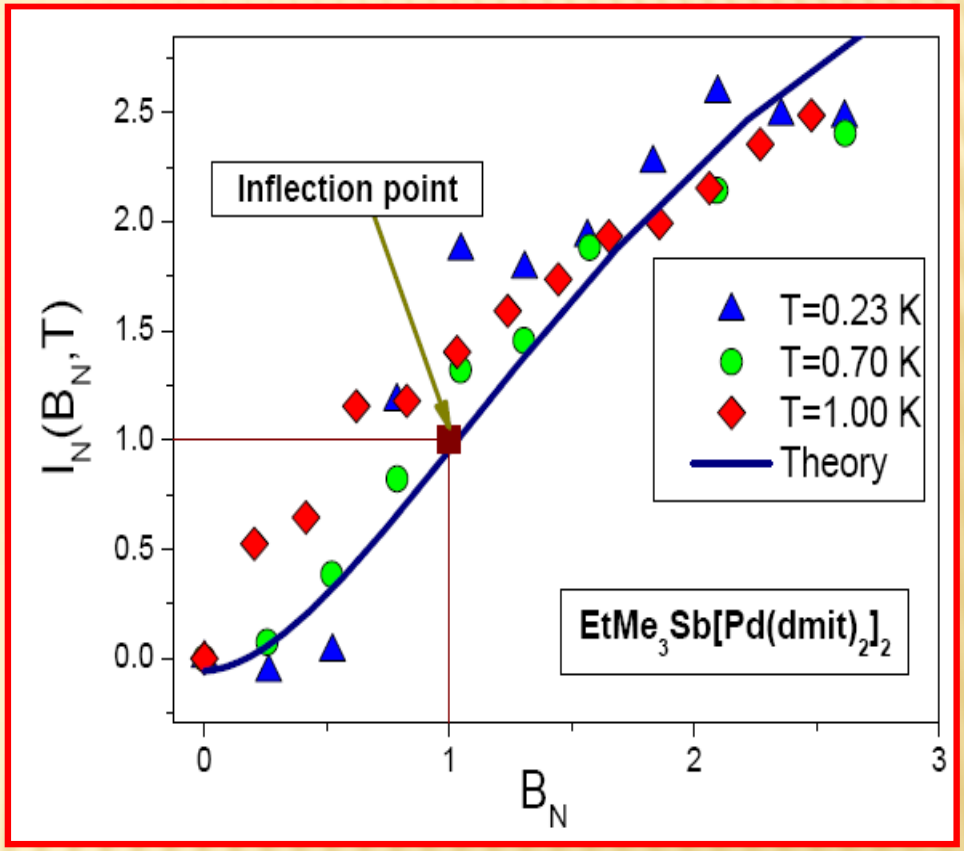

$$1 - \frac{A_w(B,T)}{A_w(0,T)} = 1 - \left(\frac{M^*(B,T)_{\rm mag}}{M^*(0,T)_{\rm mag}}\right)^2$$
$$\simeq a(T)\frac{\kappa(B,T) - \kappa(0,T)}{\kappa(0,T)} \equiv a(T)I(B,T),$$

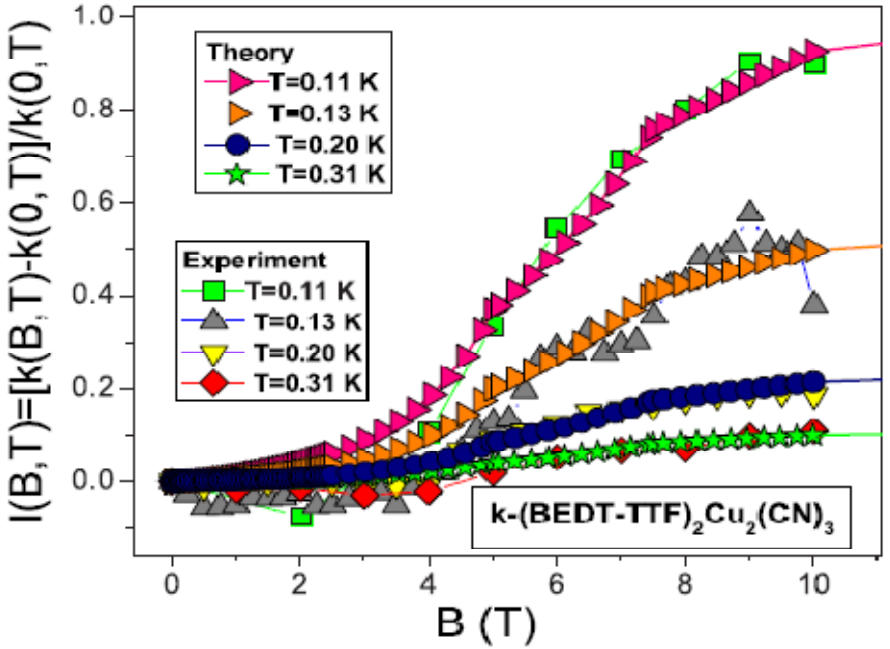

FIG. 14: Magnetic field B dependence of normalized thermal conductivity $I(B,T)$ measured on the organic insulator $\kappa-(\mathrm{BEDT-TTF})_2\mathrm{Cu}_2(\mathrm{CN})_3$ and standardized by the zero field value κ, $I(B,T)=[\kappa(B,T)-\kappa(B=0,T)]/\kappa(B=0,T)$ at temperatures shown in the legend [51]. Our calculations are based on Eq. (14) and shown by geometrical figures as it is displayed in the legend.

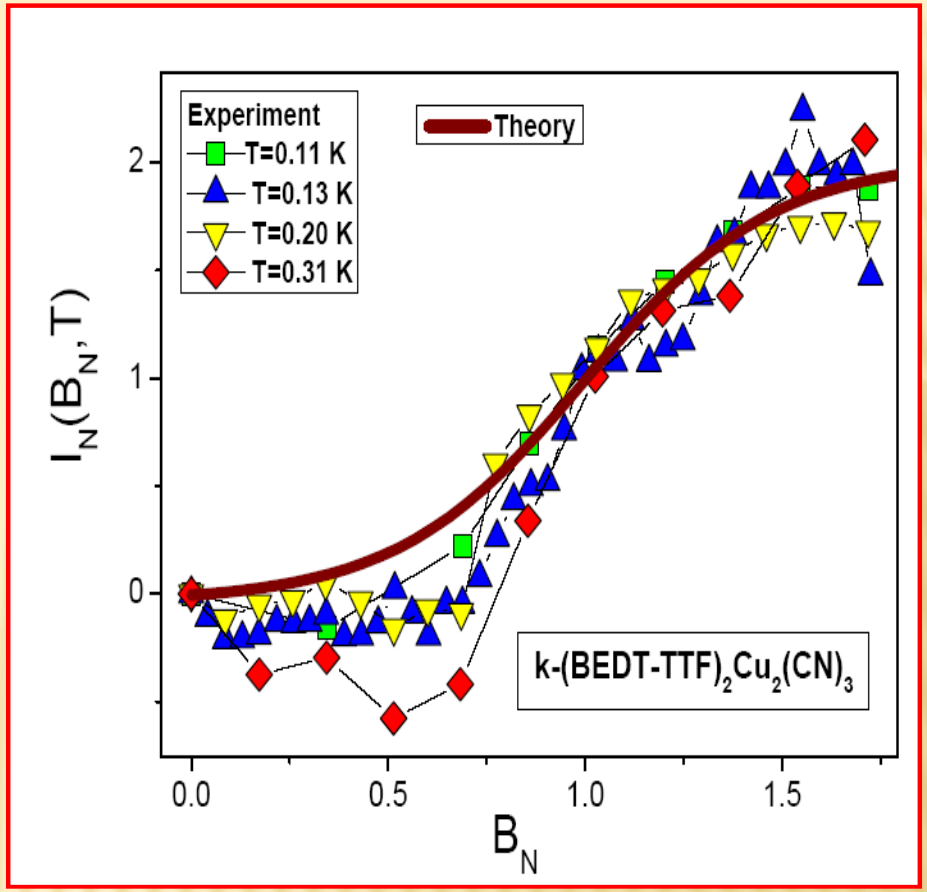

$$1 - \frac{A_w(B,T)}{A_w(0,T)} = 1 - \left(\frac{M^*(B,T)_{\mathrm{mag}}}{M^*(0,T)_{\mathrm{mag}}}\right)^2$$
$$\simeq a(T)\frac{\kappa(B,T)-\kappa(0,T)}{\kappa(0,T)} \equiv a(T)I(B,T),$$

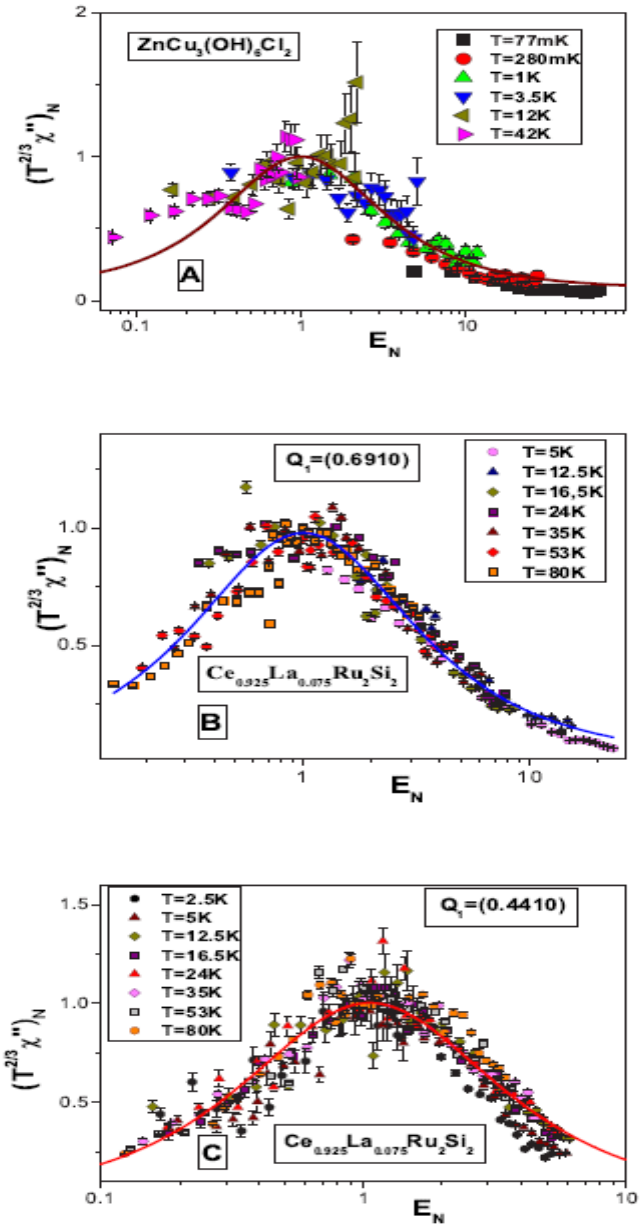

FIG. 2: (color online). The function $(T^{2/3}\chi'')_N$ plotted against the unitless ratio $E_N = \omega/((k_B T)^{2/3} E_{\max})$. The data extracted from measurements on $ZnCu_3(OH)_6Cl_2$ obtained for $0.077 < T < 42$ K [7], Panel A, and on the HF metal $Ce_{0.925}La_{0.075}Ru_2Si_2$ obtained for $2.5 < T < 80$ K at Q_1 [24], Panel B and C, collapse onto a single curve. The solid curves are fits with the function given by Eq. (9).

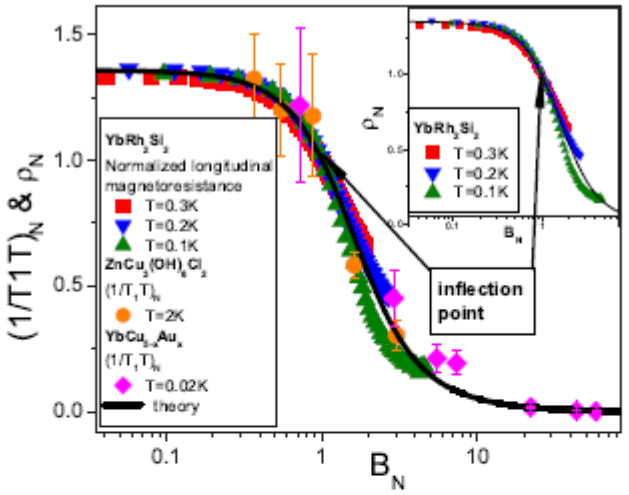

FIG. 3: (color online). Magnetic field dependence of normalized (see text for details) muon spin-lattice relaxation rate $(1/T_1T)_N$ extracted from measurements on $YbCu_{4.4}Au_{0.6}$ [28] and $ZnCu_3(OH)_6Cl_2$ [29] along with the normalized longitudinal magnetoresistance ρ_N versus normalized magnetic field B_N. Our calculations are shown by the solid line. The arrows indicate the inflection points. Inset: ρ_N versus B_N, ρ_N is extracted from measurements on $YbRh_2Si_2$ at different temperatures [30] listed in the legend. The solid curve represents our calculations.

$$\rho_N(B_N) = \frac{\rho(B_N) - \rho_0}{\rho_{inf}} = \left(\frac{1}{T_1 T}\right)_N = (M_N^*)^2$$

$$(T^{2/3}\chi'')_N \simeq \frac{b_1 E_N}{1 + b_2 E_N^2}$$

$$E = \omega/(k_B T)^{2/3}$$

Shaginyan et al., Physics Letters A 376 (2012) 2622.

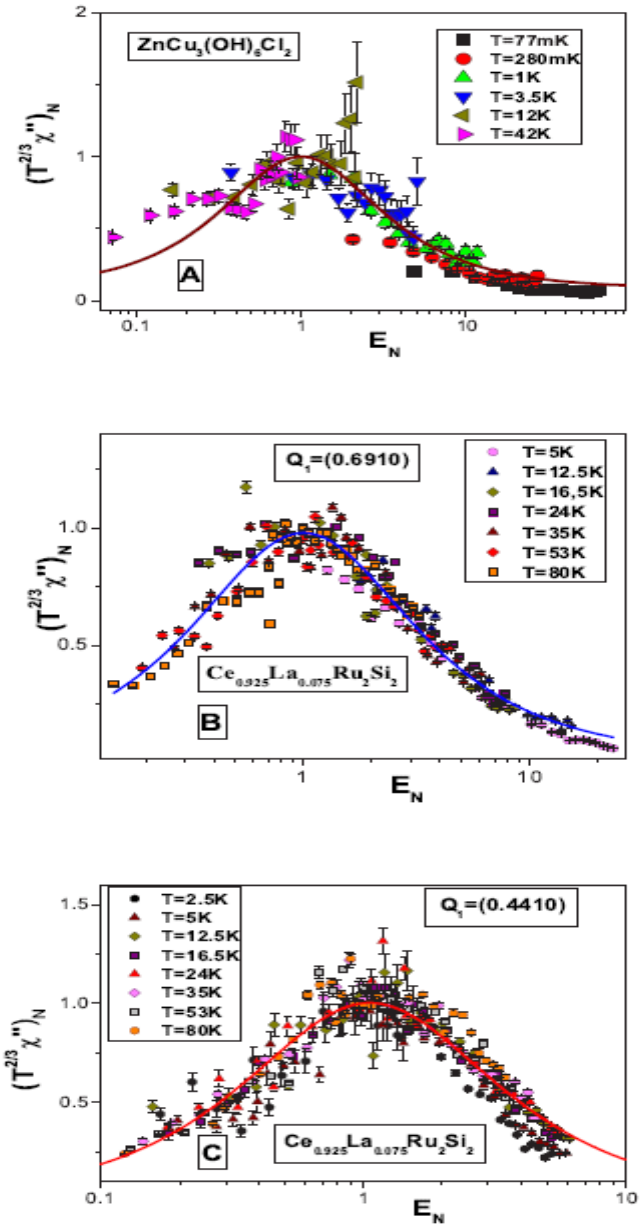

FIG. 2: (color online). The function $(T^{2/3}\chi'')_N$ plotted against the unitless ratio $E_N = \omega/((k_BT)^{2/3}E_{\max})$. The data extracted from measurements on $ZnCu_3(OH)_6Cl_2$ obtained for $0.077 < T < 42$ K [7], Panel A, and on the HF metal $Ce_{0.925}La_{0.075}Ru_2Si_2$ obtained for $2.5 < T < 80$ K at Q_1 [24], Panel B and C, collapse onto a single curve. The solid curves are fits with the function given by Eq. (9).

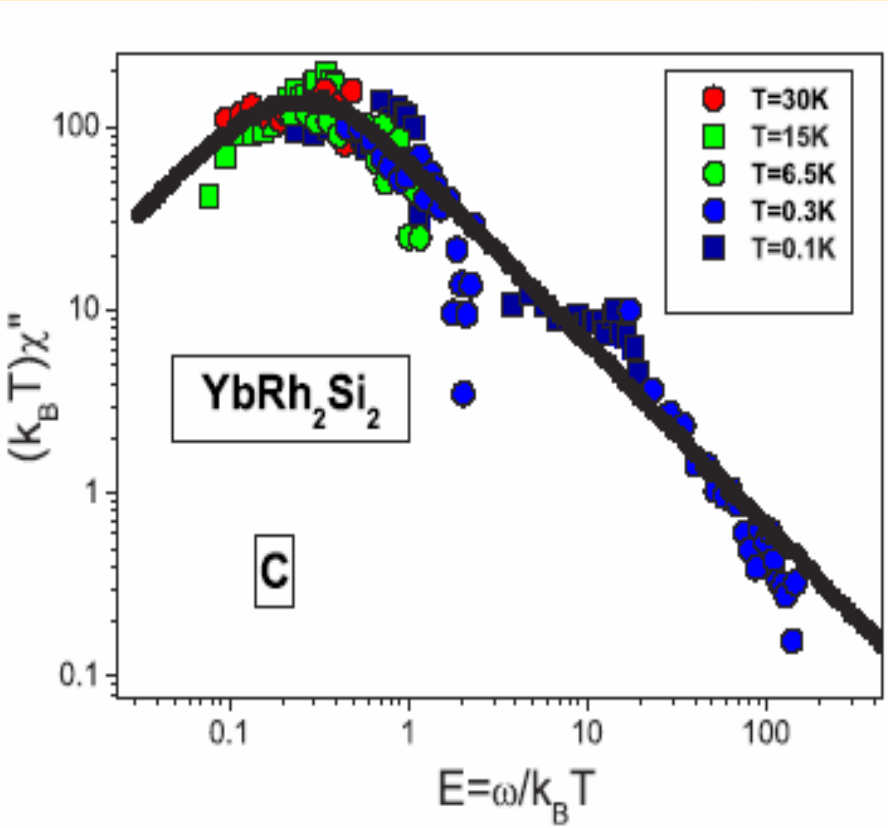

$$T\chi''(T,\omega) \simeq \frac{a_5 E}{1+a_6 E^2},$$

$$E = \omega/k_B T.$$

$$(T^{2/3}\chi'')_N \simeq \frac{b_1 E_N}{1+b_2 E_N^2}$$

$$E = \omega/(k_B T)^{2/3}$$

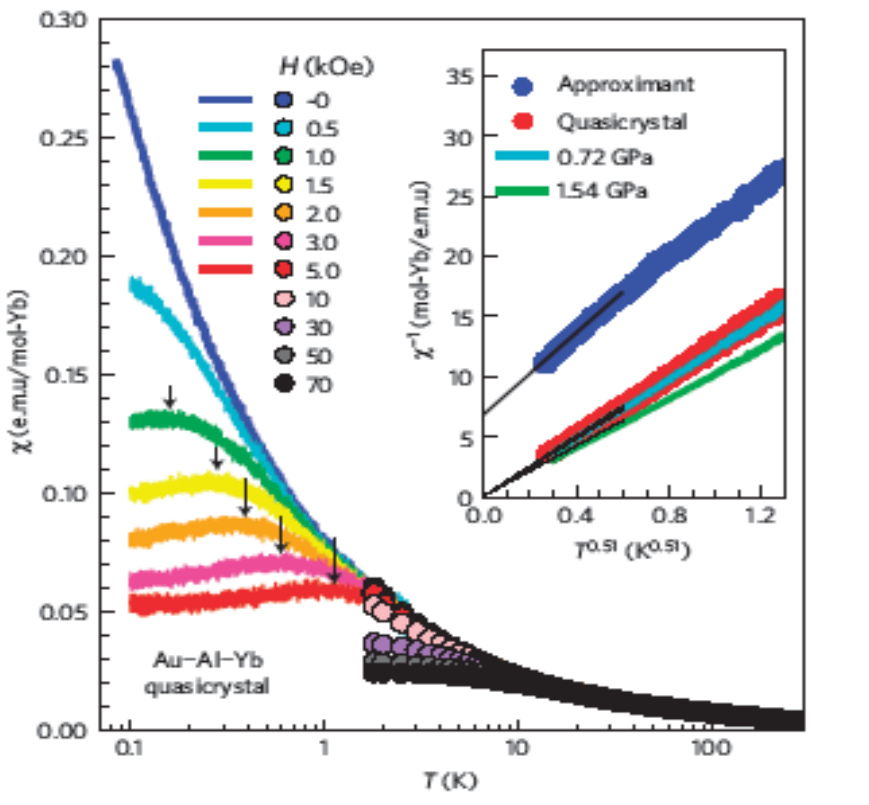

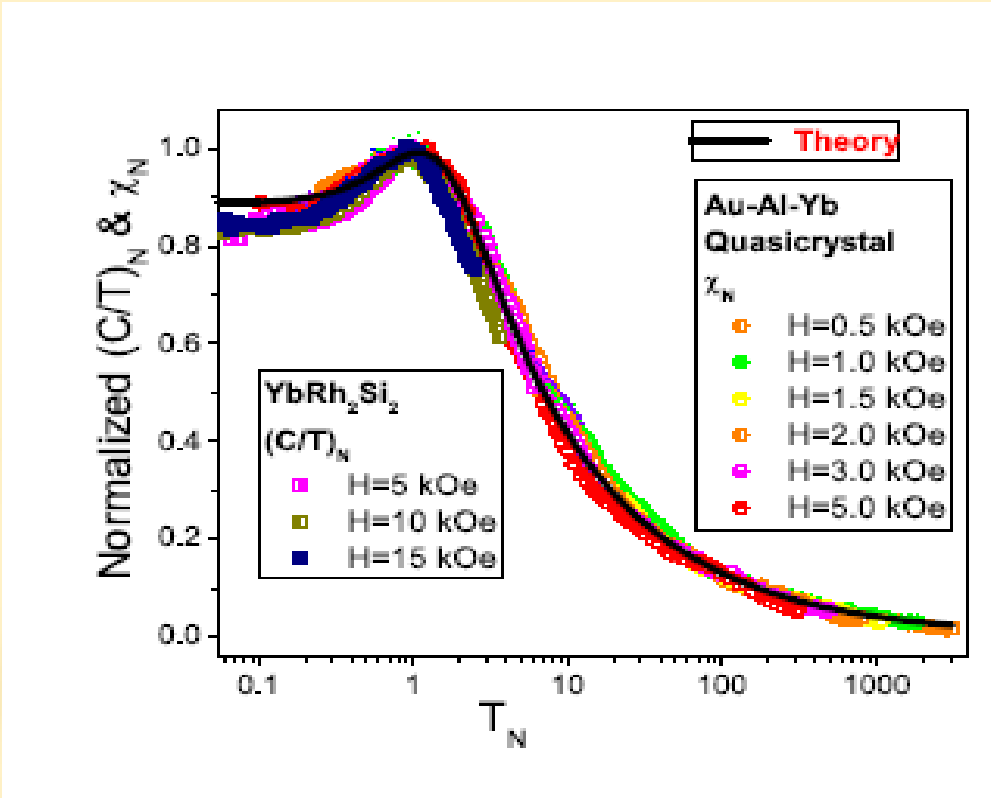

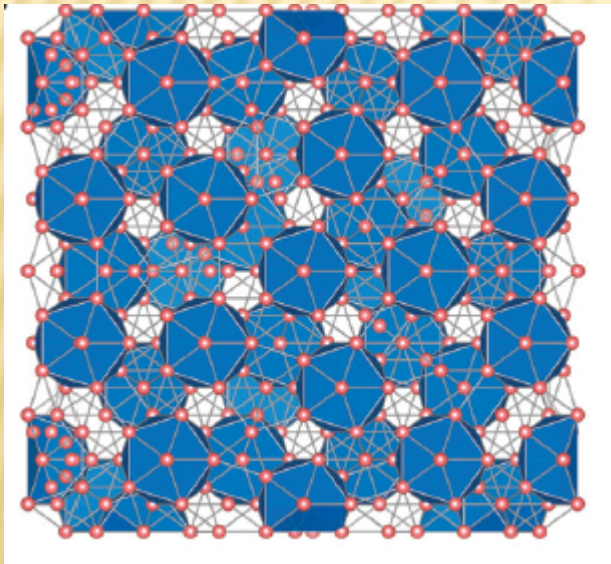

Kazuhiko Deguchi et. al., Natures materials, “Quantum critical state in a magnetic quasicrystal” (2012)

V. R. Shaginyan, A. Z. Msezane, K. G. Popov, G. S. Japaridze, and V. A. Khodel, Phys. Rev. B **87**, 245122 (2013).

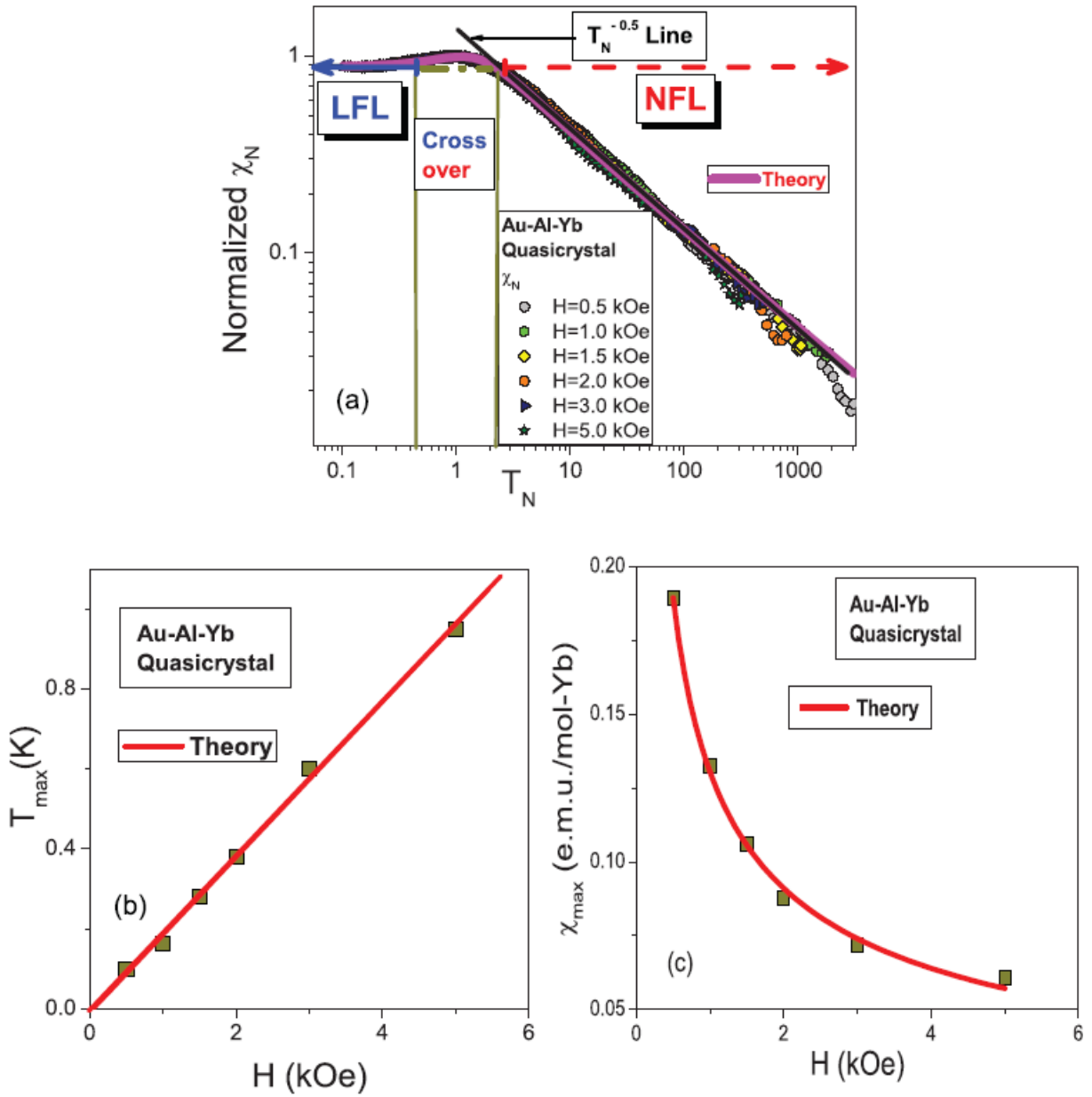

FIG. 3. (Color online) (a) Temperature dependence on the double logarithmic scale of the magnetic susceptibility χ_N at different magnetic fields (Ref. 9) shown in the legend. The LFL region and NFL one are shown by the solid and dashed arrows, respectively. The solid line depicts $\chi_N \propto T_N^{-0.5}$ behavior. (b) The temperatures $T_{\max}$ at which the maxima of χ (see Fig. 1) are located. The solid line represents the function $T_{\max} = aH$; a is a fitting parameter. (c) The maxima $\chi_{\max}$ versus magnetic field H. The solid curve is approximated by $\chi_{\max} = tH^{-1/2}$, see Eq. (9); t is a fitting parameter.

Our calculations unveil the fundamental properties of QSL, forming strongly correlated Fermi system located at FCQPT. The key features of our findings are the presence of spin-charge separation and QSL formed with itinerant heavy spinons in herbertsmithite. Herbertsmithite represents a fascinating experimental example of strongly correlated insulator when the new particles - spinons, non-existing as free ones, totally replace the initial particles entering the Hamiltonian to dominate the properties at low temperatures.

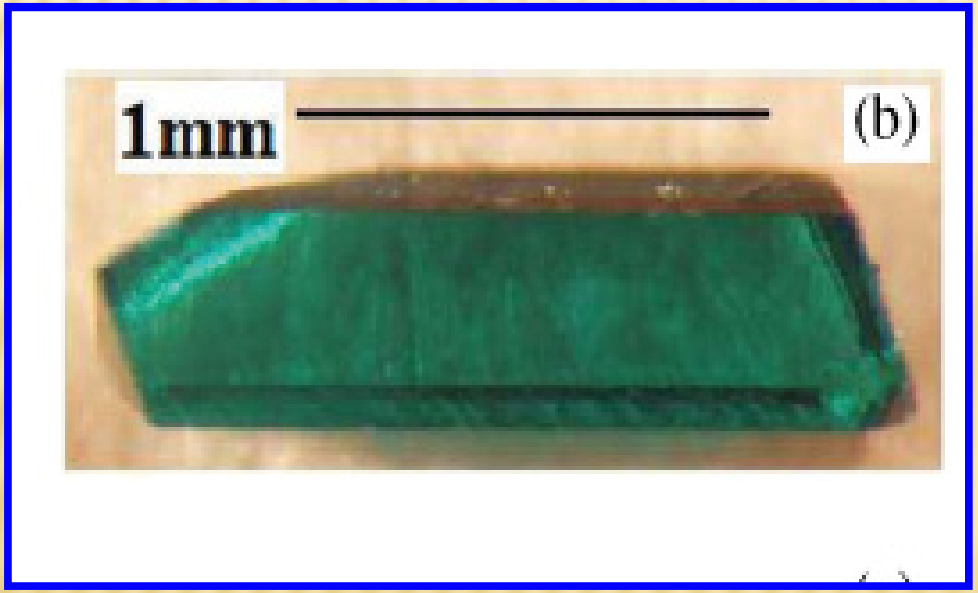

SUMMARY

Insulators with QSL represent a a new type of strongly correlated electrical insulator that possesses properties of heavy fermion metals with one exception: it resists the flow of electric charge.

Herbertsmithite is a fascinating experimental example when new particles-spinons, non-existing as free ones, dominate its properties at low temperatures.

We have also demonstrated that the insulators with QSL exhibit the Landau Fermi-Liquid, Non-Fermi Liquid and the transition behavior as HF metals and 2D 3He do.

Our calculations of the thermodynamic and relaxation properties are in good agreement with the experimental facts and their scaling behavior coincides with that observed in HF metals, 2D 3 He, and quasicrystals.

Caused by the spin-charge separation the low-temperature thermodynamic, heat transport and relaxation properties of the insulators with QSL are similar to those of metals rather than of insulators.

Thank you for your attention!